Master's Thesis - master Energy Science

Floating PV systems: assessing ecological and economic impacts of Floating photovoltaic systems on in-land waters.

A case study of Zonnepark Beilen, using a thermodynamic approach complemented by computational fluid dynamics.

Niek van den Nobelen

A thesis presented for the degree of
Energy Science

Supervisors:
Dr. Sara Mirbagheri Golroodbari
Annanta Kaul

Second assessor:
Prof. dr. Wilfried van Sark

Faculty of Geosciences
Utrecht University
The Netherlands

December 20, 2023

Abstract

Around the world countries are working on the transition from a fossil fuel-based energy supply towards more sustainable energy generation by for example means of wind and solar. This is also the case for the Netherlands, one of the leaders in implementing photovoltaics for energy generation. In recent years, Floating Photovoltaic Energy (FPV) systems show a notable increase in the Netherlands, reaching an installed capacity of 230 MWp by the end of 2022. Due to the novelty of this technology and increased complexity compared to their ground-mounted counterparts, its long-term effects on the environment are not fully mapped. In addition, costs of implementing FPV systems are higher as additional hardware like flotation devices and more complex cabling are required. This thesis features a case study of Zonnepark Beilen located in the Netherlands. The thesis assesses the thermal impacts of an FPV system on the water body, how this affects the water body's ecology, and how this affects the economics surrounding FPV systems and local businesses. The method combines Computational Fluid Dynamics (CFD) with a thermodynamic model to determine heat transfer dynamics based on the available dataset of Zonnepark Beilen. The results are combined with a literature study focusing on ecological impacts induced by the FPV system. The ecological impacts and implications of the altered thermal system of the water body are translated into economic opportunities for businesses related to water bodies. The results of this thesis show that heat transfer dynamics are for a large part dependent on wind speeds underneath the installed modules, which vary greatly depending on the position of the module in the FPV system, where wind speeds are lower the further it has progressed underneath the system. Installing an FPV system has a slight, year-round, cooling effect on the water body. This effect, combined with the reduced wind speeds underneath the system affects the local ecology in various ways. Lower wind speeds and reduced sunlight lower the concentration of algae underneath the FPV system compared to open water areas. Lower wind speeds also reduce water evaporation. Dissolved oxygen values, important for marine life see little to no impact for Zonnepark Beilen, however, this might be the result of the water body being an open system. These effects in general, improve water quality which is beneficial for businesses related to water bodies such as; water treatment plants, fish-spawning, and sports fishing facilities. Results of this thesis contribute to a better understanding of heat transfer dynamics between FPV systems and water bodies, in addition, wind dynamics surrounding the FPV system can provide useful insights into the system's performance and thermal distribution. The ecological trends resulting from the changes provide a positive outlook for FPV systems as no notable complications occur, albeit that long-term effects remain unknown until further observations are done.

Contents

Abbreviations

PV	Photovoltaic
USSE	Utility Scale Solar Energy
FPV	Floating Photovoltaic Energy
GPV	Ground mounted Photovoltaics
CAPEX	Capital Expenditures
OPEX	Operational Expenditures
LCOE	Levelized Costs of Energy
CFD	Computational Fluid Dynamics
NHI	Net Heat Input
O&M	Operation and Maintenance

Symbols

A	Area
α	Albedo
Ghi	Global irradiation
$Gpoa$	Plane of array irradiance
H_c	Sensible heat
H_e	Latent heat
H_{br}	Background radiation
K	Thermal conductivity of air
L_v	Latent heat of vaporization
$Nu_{\text{free, forced}}$	Nusselt numbers for free and forced convection
$Q_{\text{B, conv}}$	Convective heat transfer for back sheet
$Q_{\text{B, rad}}$	Radiative heat transfer for back sheet
R_{sw}	Shortwave
RH	Relative humidity
σ	Stefan-Boltzmann constant
T_{amb}	Ambient temperature
T_b	Temperature on the back of the module
T_{ws}	Water surface temperature
T_w	Water temperature
U	U-value
U_C	U-value constant
U_v	Wind dependent U-value
v_w	Windspeed
ε_{bw}	Emissivity from back sheet to the water surface
ε_{ws}	Emissivity of the water surface
η	Efficiency
ϕ	View factor
$h_{\text{c back}}$	Convective heat transfer coefficient for back sheet
$h_{\text{c forced}}$	Forced convection heat transfer coefficient
$h_{\text{c free}}$	Free convection heat transfer coefficient
ρ_a	Density of air

List of Tables

List of Figures

1 Introduction

1.1 Societal background

For many countries, the energy transition is a prominent point on the political and public agenda. Continuous efforts are made every year to move from the incumbent fossil-based energy system towards a sustainable energy system free from greenhouse gas emissions. Within the energy transition, solar Photovoltaic (PV) has become one of the most popular renewable energies by accounting for 60% of the total added renewable capacity in 2022 (IEA, 2022). The substantial increase in solar PV implementation can be seen in the Netherlands, where installed capacity increased by 28% in 2022 compared to the previous year, achieving 1044 watts/capita. This makes the Netherlands the frontrunner of the EU in 2022 regarding solar PV implementation (CBS, 2023). While the increase of solar PV technologies is crucial for the energy transition's success, the effects of Utility Scale Solar Energy (USSE) have not been studied that well throughout the years. For instance, USSE in densely populated countries are often installed on arable land or land that is suitable for agricultural exploitation or forestry. Additionally, cleaning lands already occupied by crops or other vegetation for USSEs had additional consequences like impacts on biodiversity, carbon cycling, and aesthetics (Ven et al., 2021). Looking at the Netherlands, a country with a population density of 522 people per km^2, the problems of USSE and other stakeholders for usable plots of land are also present (Nations, 2022; Zomerdijk, 2018). From 2021 to 2022, the Netherlands has seen a growth in installed PV capacity of 22% indicating that PV is still increasing even with the aforementioned competition (CBS, 2023). It is expected that in the coming years, the competition, as well as the prices for plots of land suitable for USSEs, will increase. For example, in 2021/2022, the price for agricultural land has increased by 5.8% and is likely to increase further as demand increases (Kadaster, 2023).

A relatively new trend in the surge of global installed PV capacity is Floating Photovoltaic Energy (FPV) systems, which have experienced a doubling growth rate from 2015 and onward (Gorjian et al., 2021). FPV systems use in-land or off-shore water bodies to generate electricity from solar irradiation. Therefore, large-scale FPV systems do not take up valuable patches of usable land while generally being able to scale up to larger installations compared to land-based systems (Folkerts et al., 2017). Additionally, FPV systems have extra benefits like increased PV efficiency due to cooling effects, lower module degradation, reduced water evaporation, less dust accumulation, and water quality improvement (Essak and Ghosh, 2022; Gorjian et al., 2021; Kumar et al., 2021). At present, China leads in installed FPV capacity, accounting for 75% of the total, followed by Japan in second place with 15% of the installed capacity. Despite the vast global potential for FPV systems, their implementation is still lacking in widespread adoption worldwide. With increasing land prices and the scalability potential of FPV systems, this technology might provide an alternative for installing sustainable energy systems in the Netherlands, where, as mentioned above, the land is scarce, and FPV systems could prove to be economically viable. The Netherlands has roughly 52.000ha of shallow water bodies that are suitable for FPV system implementation and, therefore, lots of potential for large-scale FPV implementation (Kumar et al., 2021). Progress with implementing FPV systems in the Netherlands has already been made. Several FPV systems of varying sizes on both in-land and open-water bodies have been realized, some being capable of powering up to 4,000 households

(GroenLeven, n.d.). According to TNO (n.d.) some scenarios expect a possible installed FPV capacity of 70GWp by the year 2050, again showing the potential of FPV systems in the Netherlands. As of 2022, 230MWp of FPV capacity has been installed in the Netherlands (Solar 365, 2023)

1.2 Scientific background

The success of solar energy in the global energy transition has led to multiple directions in the technology's development. On the one hand, efforts are put into increasing cell efficiency through optimized production or developing new PV technologies. On the other hand, research pathways focus on the implementation phase of PV systems, with one notable approach being FPV systems (Khokhar et al., 2020). As mentioned before, FPV systems solve the issue where countries have limited free land available but still want to increase the share of renewable energy in their energy mix.

In the field of FPV systems, there are two main categories to differentiate in: Off-shore FPV systems and In-land FPV systems. Both technologies follow the same principle: solar panels are mounted on floating devices like bridges, pontoons, or inflatables. The buoyant devices are then anchored to the ground and connected to land with a cable to transfer the generated power to a substation for further distribution (Golroodbari et al., 2022). Regarding the in-land application of FPV systems, various types of water bodies are suitable for implementation and potentially serve a dual purpose, like irrigation ponds, wastewater treatment, fish farms, and dams. This means that even if the FPV systems occupy the water surface, the water body can still be operational for other exploitation.

Due to FPV being a relatively new technology, much research is still required regarding the environmental impacts of FPV systems on the targeted water bodies. (Ilgen et al., 2023) and (Exley et al., 2021) are examples of studies highlighting the environmental changes and the impacts that might occur. Effects during the implementation phase of an FPV system are perceived as relatively constant and relate mainly to reduced light irradiation, evaporation, and water surface wind speeds. For the ecology of the lake surrounding the system, reduced sunlight irradiation is deemed to have one of the largest impacts on fauna and microbial life as reduced sunlight results in lower oxygen production by photosynthetic organisms in the water, impacting oxygen-depending organisms (Silva and Branco, 2018).

A downside of FPV system, which is an important reason for the lower implementation rate, is the increased costs that FPV systems have compared to Ground mounted Photovoltaics (GPV) systems (Golroodbari et al., 2022; Essak and Ghosh, 2022; Kumar et al., 2021). For example, Gorjian et al. (2021) determined that for a hypothetical 50MWp PV installation, the Capital Expenditures (CAPEX) were US$ 0.73/Wp for the FPV system and US$ 0.62/Wp for the GPV system. Looking at the Operational Expenditures (OPEX), the rent for FPV systems is expected to be lower as the water surface cannot be used for other purposes like residential buildings or agricultural use. Other Operation and Maintenance (O&M) costs of a PV system are generally linked to replacing broken components in the system like PV panels or inverters and cleaning PV modules. FPV systems could pose higher O&M costs as the system contains more components (moorings, pontoons, floaters, etc.), the potential for a required cooling

system, more frequent cleaning and more expensive maintenance as the system is floating, and boats/other equipment must be used to reach the system (Gorjian et al., 2021). Looking at costs from the Levelized Costs of Energy (LCOE) perspective, FPV systems are expected to be slightly more expensive across the system lifespan than GPV systems, which provides an interesting case. CAPEX and OPEX values are highly dependent on the location and design of the systems; looking at FPV systems in densely populated countries could prove to be economically more interesting as land is more expensive, and O&M costs could drop due to, for example, intelligent system design. While various aspects of FPV are already subjected to thorough research projects, some gaps in the literature still remain. These will be discussed in the following section.

1.3 Case study, Problem definition, and research questions

FPV systems are a promising application for an already mature technology. However, the increased systems costs compared to GPV systems and lack of knowledge on impacts halts the deployment rate of the technology. While the environmental impacts, performances, and economics of FPV systems have been investigated by researchers, there has been little research regarding business opportunities for in-land water body operations like food production. These businesses often require electrical power, and the changes that FPV systems bring to the physiological and ecological aspects of a water body can potentially benefit business operations. Through analyzing the potential thermal impacts on the water body of the FPV system, environmental impacts, and economic aspects of water-related businesses, a techno-economic view used to determine whether FPV systems provide economic benefits to in-land bodies of water. Therefore, this thesis aims to answer the following research question:

What are the added economic benefits of an FPV system for businesses that are reliant on in-land water bodies and how are these, in turn, beneficial for FPV implementation?

Several sub-research questions have been established to guide the research and report interim results:

1. *What are the thermodynamic effects of FPV systems on in-land water bodies?*
2. *How do these effects translate into environmental impacts in the water body?*
3. *How do these thermodynamic and environmental effects translate to economic impacts for businesses?*

The thesis will be conducted in the form of a case study for an FPV system located in Beilen, the Netherlands. GroenLeven has implemented the system, which is hereafter referred to as: "Zonnepark Beilen". Conducted methods and generated results, therefore, will focus on the aspects of Zonnepark Beilen but will also be put into a broader context.

While executing the proposed research method, it became clear that with the proposed method and acquired data, the results of the thermodynamic model would lack accuracy. Due to the unavailability of data for wind speeds below the solar panels, an additional step in the research methodology has been added which focuses on Computational Fluid Dynamics (CFD) to analyze wind speeds and wind dynamics. Establishing, executing and processing the CFD

analysis required a lot of time and effort but yielded valuable results. The decision to pursue the CFD analysis resulted in the choice to put less time into the ecological and economic impacts, having the result that these subjects are only addressed qualitatively. The research questions will remain unchanged, yet while concluding this thesis project; more attention is paid to answering sub-research question 1 than the rest.

This paper will first present the theoretical background for concepts and methods used in the project in section 2; this is followed by the proposed method to generate results and insights in section 3. The paper features four sections discussing the results of each step proposed in the methodology in section 5, section 6, section 7, and section 8 Finally, the paper concludes by discussing the results and applied methods in section 9 and by answering the main and sub-research questions in section 10.

2 Theoretical background

This research explores business opportunities created by introducing an FPV system to a Dutch in-land water body via a techno-economic analysis. The analysis uses thermodynamics, physics, computational fluid dynamics, and ecology to assess these opportunities. This chapter provides an overview of the scientific concepts supporting the project.

2.1 Electrical performance

Research into accurately modelling the performance of **GPV!** setups is well-established, similar principles apply to FPV. In this case, the performance of a solar array is determined as the DC output power and is calculated by multiplying the array's current by the voltage. The power conversion efficiency from solar energy to electric energy ranges up to 26.8% for the top-of-the-range silicon-based PV cells under Standard Test Conditions (STC)[1] (Green et al., 2023). In general, PV cell efficiency tends to decrease when the cell temperature (T_{cell}) increases due to augmented electron mobility and decreased voltage. Figure 1 shows the dependency of a monocrystalline PV cell and the change in the power output when (T_{cell}) is increased.

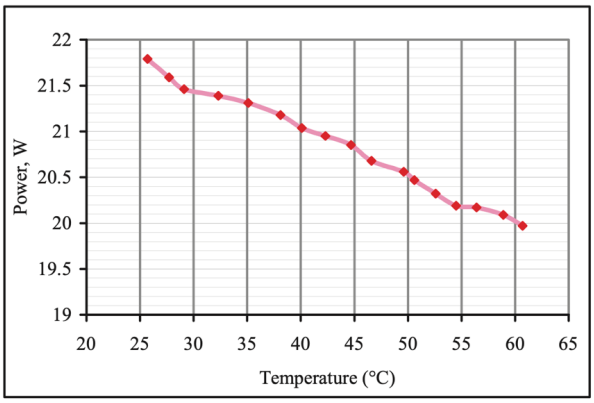

Figure 1: Change in power output of a monocrystalline solar panel with increasing temperature. (Zaini et al., 2015)

With the presence of water near the PV modules, a cooling effect is introduced to the system, decreasing the module's (T_{cell}) and increasing the power output. An example of the potential cooling effect is given in Figure 2. Figure a shows the different performance ratios between air and water called PV systems. Additionally, the yield differences are shown in figure b, highlighting the increased effect in the generally warmer months compared to months where environmental temperatures are lower. This thesis will incorporate the added cooling effect into the performance analysis to determine the added benefits for the system considered for this project.

[1] STC is defined as 1000W/m^2 of solar irradiance, 25°C cell temperature and an airmass equal to 1.5 (Elkholy and El-Ela, 2019).

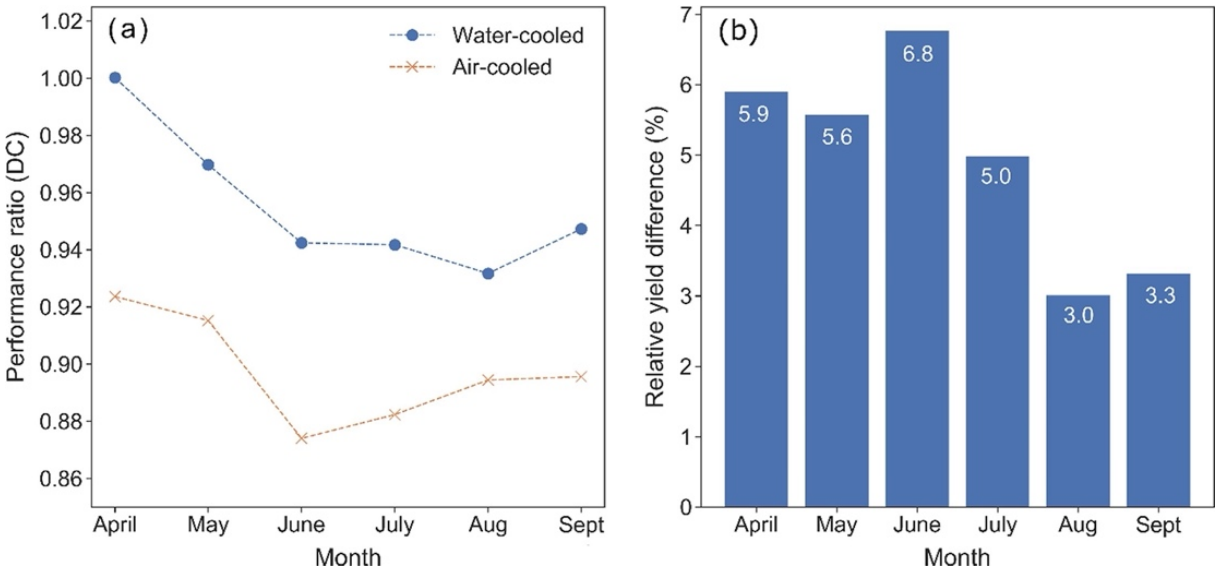

Figure 2: Visualization of beneficial cooling effects when PV systems are cooled by water compared to air-cooled PV systems. (Kjeldstad et al., 2021)

2.1.1 Computational Fluid Dynamics (CFD)

The field of CFD focuses on simulating the behaviour of fluids on multiple aspects like heat transfer, flow speeds, turbulence, and force distribution. This modelling approach aims to generate real-life results of how fluids like water and air will behave around mechanical structures for validation purposes. CFD computation is based on Navier-stokes equations in three dimensions to determine the relation between velocity, temperature, pressure, and density of a moving fluid (NASA, 2021). Since the emergence of FPV systems, several researchers have applied CFD to various existing arrays and array configurations. For example, Lindholm et al. (2022) have used CFD to assess the heat loss of FPV systems by wind speeds and water temperatures. Chowdhury et al. (2023) present their findings on multiple metrics on the impacts of wind speeds, temperatures, and tilt angles of FPV systems and draw various conclusions regarding the cooling of the surroundings on the floating system. Both papers present interesting findings about heat exchange and cooling effects on relatively small-scale CFD simulations. However, CFD analysis on larger scale systems is not well-represented in current literature and can provide additional insights on how wind speeds develop underneath floating arrays and, thus, how cooling effects change. Assessing these effects and applying the results of CFD analyses to a heat-transfer model can provide more accurate results for large-scale FPV utilities than single-row or panel-by-panel simulations

2.2 Thermodynamic modelling

FPV systems are subjected to various thermal flows bringing and extracting heat from the array into the surroundings. For the scope of this thesis, the focus is on the thermal impacts that the solar array has on the water temperature of the water body. The abstract of Golroodbari and Sark (2023), describes the thermal dynamics of an FPV system that is introduced to an in-land body of water and identifies the change in incoming short-and-long wave radiation

as the main reason for thermal differences in the water body this dynamic is described by the Net Heat Input (NHI). In addition to the heat inputs, the water body also loses heat through convection and evaporation, which are both affected by installing an FPV system. In their paper, Rahaman et al. (2023) presents a holistic method of assessing the thermodynamic interactions between an FPV system and the water body temperature. Additionally, the paper mentions that evaporation, solar irradiation, and wind speeds are the most critical factors regarding water temperature changes.

2.3 Environmental impact assessment

The ecological footprint of FPV systems remains largely uncertain. Numerous studies have analyzed the impact of FPV on water bodies, highlighting effects such as reduced evaporation and algae bloom, as well as shifts in temperature, light, and wind (Ilgen et al., 2023). Despite potential drawbacks, these changes could also be harnessed beneficially for economic activities, such as water treatment plants (Exley et al., 2021). Assessing FPV system effects is complex due to the diverse ecological metrics available. This research focuses on metrics reflecting altered water temperatures. Water temperature impacts evaporation and ecological processes, influenced by solar irradiance and seasonality (Exley et al., 2021; Ji et al., 2022). These aspects in turn are influenced by the presence of FPV systems that block incoming sun and alter the wind flow across the water.

2.4 Marine food production

The global warming effect has impacts on both oceans and inland water bodies. Increasing temperatures result in a decrease in volume due to evaporation in the lower latitude regions, but lakes located at higher latitudes are expected to increase in volume due to increased precipitation and molten ice flows (Cochrane et al., 2009). The increased temperatures influence the level of nutrient and microbial life composition of the lakes (either increasing or decreasing) which has various impacts on the so-called "blue food" supply chain (Cao et al., 2023). Reduced water volume and increased aqua cultural activity also pose a risk for algae blooms that thrive on increased nutrient concentrations in a process called eutrophication (excessive increase of nutrients like nitrogen and phosphor in water bodies), killing fish in the process (Ahmed et al., 2019). In addition to the risk that climate change imposes on the productivity and yield of aquaculture, the sector's sustainability is relatively low. Figure 3 shows multiple metrics for fish production on a global level. One of the notable metrics is Figure 3.f showing that the carbon productivity of fish production in Europe is roughly between 0.005$ and 0.010$ per tonne of CO_2 emitted (Jiang et al., 2022). For comparison, the carbon productivity of beef is roughly 51.91$ per tonne CO_2 emitted[2]. Representing added value per unit of greenhouse gases emitted. Introducing FPV systems to fish breeding facilities can potentially increase numerous metrics shown in Figure 3.

[2]Carbon productivity of beef is determined by dividing the average price for one tonne of beef (5140$ at the time of writing) (Statista, 2023b) with the emissions tonne CO_2 emissions/tonne beef (99.0) (Statista, 2023a).

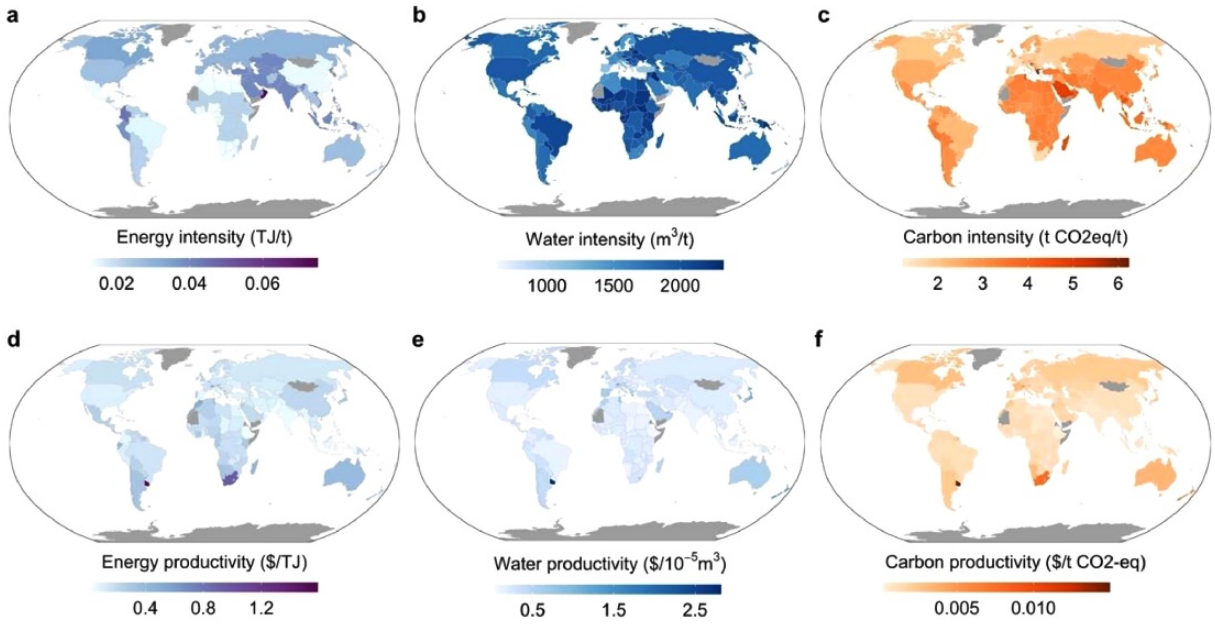

Figure 3: Several figures highlight different metrics of aquacultural impacts in various world regions. (Jiang et al., 2022)

3 Methodology

A multi-step approach has been applied to assess the impacts that an FPV system has on the thermodynamics and ecology of an in-land water body, with the main idea visualized in Figure 4. The method has been established to focus on generating insights regarding the thermodynamics of FPV systems, which, in turn, will be used to answer the research questions highlighted in the section: Case study, Problem definition, and research questions. The method will be used as a case study for Zonnepark Beilen, located in the Netherlands. This location has been studied in this thesis due to the data availability made possible by Groenleven. The methodology flow shows how the data from Zonnepark Beilen will serve as an input for both the CFD analysis and the thermodynamic analysis. Additionally, results from the CFD analysis will also be used for the thermodynamic model. The results from both models will then be used for further research regarding the impacts of the system at Zonnepark Beilen. In this chapter, the applied method will be discussed in more detail.

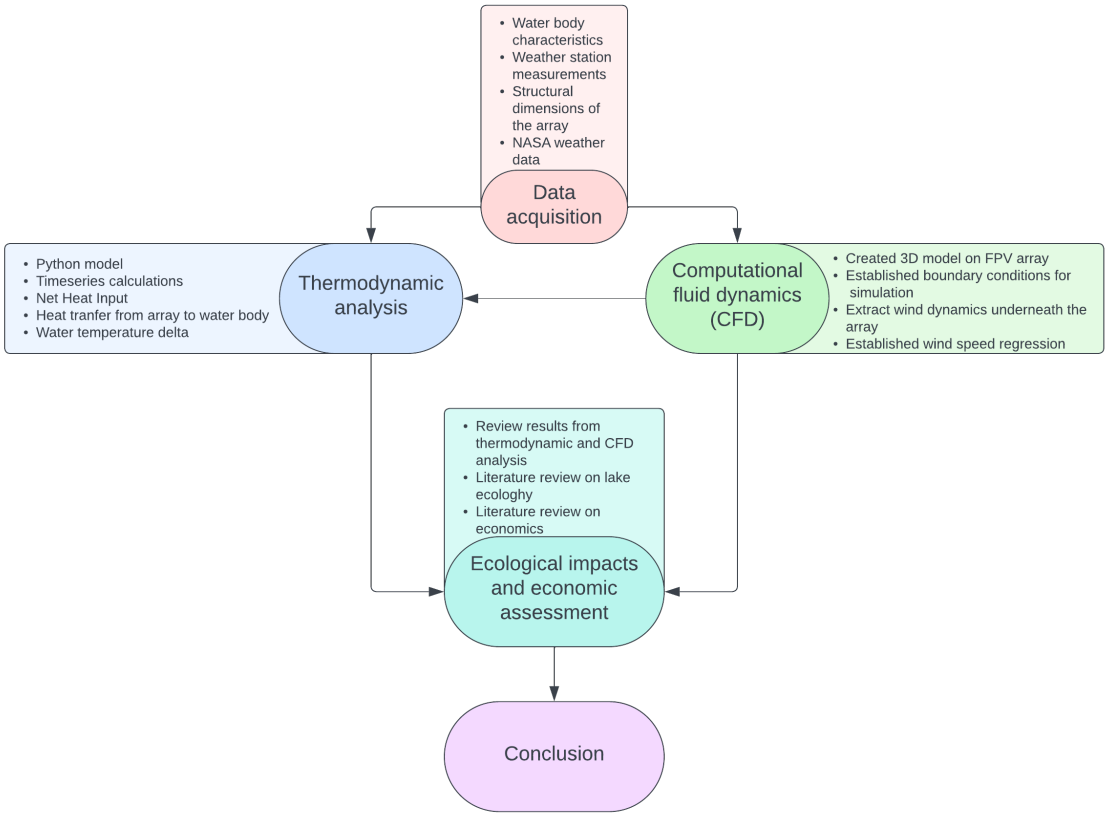

Figure 4: Schematic overview of the methodology flow

3.1 Data acquisition

This section elaborates on how required data implemented in the method will be acquired. First, the data required for the CFD analysis and thermodynamic analysis will be discussed, followed by the strategy for the ecological and economic impact data.

3.1.1 CFD and thermodynamic modelling data

For the thermodynamic analysis, a dataset of Zonnepark Beilen has been made available by Groenleven. The dataset contains roughly 2 years' worth of data, featuring measurements of wind speeds, wind direction, ambient temperature, power output, tilt angle irradiance, and module temperature. These measurements were taken on two different points at the array and showed no notable differences. In addition to the dataset from Groenleven, data on the local relative humidity (RH) has been gathered from NASA's database. This dataset features the relative humidity for one square kilometer at the exact latitude/longitude as Zonnepark Beilen. Both datasets have been processed in a Jupyter notebook environment, scanning for missing data entries and unrealistic values (e.g. ambient temperatures $\geq 100°C$ and similar). Missing or unlikely values have been imputed and replaced with interpolated values. These interpolation measures vary from inserting a rolling average to linear interpolation.

For the CFD analysis, wind speed, wind direction, and temperature data from the dataset have been used to initiate the boundary conditions of the simulation. Additional data with information like the structural dimensions of the floaters, mounting system, and PV modules. In addition, CFD software and knowledge about how to implement the software had to be acquired in order to conduct the CFD analysis.

3.1.2 Environmental impact and economic analysis

Data on environmental impacts due to temperature changes must be acquired to interpret the results from the CFD and thermodynamic analysis. The results found in the literature will be compared against the outcomes of said analyses to get insights into how the system alters its surrounding environment and its financial implications. This has been done through desk research. In addition, the results from the CFD and thermodynamic, as well as the identified ecological impacts, will be used to determine economic impacts and benefits. To identify these impacts, desk research will be applied to look for literature or news publications reporting on these topics.

3.2 Computational Fluid Dynamics (CFD) analysis for wind effects

For the heat exchange between the back of the solar panels and the water surface, the wind speeds between the system and the water are the main contributors. Due to the absence of sub-panel wind speed measurements, CFD will be applied to assess the wind speeds underneath the FPV systems for the sake of more accurate results in the thermodynamic analysis. In addition, the shallow layout of Zonnepark Beilen gave the assumption that little wind is able to get underneath the system increasing uncertainty about using approximated or assumed wind speed values.

Using the Autodesk Fusion 360 and Autodesk CFD software, a 3D interpretation of a string has been made to represent the array as accurately as possible. The model has been based on technical drawings and video images from a similar floating array to determine the effects of the wind underneath the array as accurately as possible. Due to the computational complexity of CFD analyses, only a part of the floating array could be simulated, as implementing the full-scale design requires supercomputer-like facilities. The maximum model size that could make it through the analysis with the available computational resources features 20 strings arranged in a 5 by 4 layout featuring strings containing 18 solar panels.

The Computational Fluid Dynamics (CFD) analysis has been set to simulate a wind tunnel with the wind coming from the southwest, as this appeared to be the most observed trajectory. The boundary conditions for the analysis have been set for a variable air inlet with a wind speed of 15m/s. This means that the simulation will start with said incoming wind speed, representing the highest measured wind speeds from the dataset. This value has been chosen to simulate the strongest effect of wind dynamics underneath the array. The end of the wind tunnel has been set for a pressure region with atmospheric pressure. The side and top 'walls' were set with a slip boundary to omit viscous effects between the air and model boundary. The set number of iterations for the wind tunnel analysis is 500. However, Autodesk CFD

will stop the simulation if the convergence lines are straight, indicating that the Navier-Stokes equations are solved (NASA, 2021).

3.2.1 Two stage analysis

As mentioned prior, the size of the array is too large for the available computational power to run. However, a second simulation has been established to approximate how the wind speeds develop further than the initial analysis. This simulation has virtually the same setup as the initial simulation, albeit with different starting variables. The air inlet velocity for the second simulation has been assigned as the exit velocity from the first analysis. Second, the angle of attack has been set to be parallel to the outgoing wind direction following the first array instead of facing the wind at an angle of attack. The choice to align the wind direction parallel to the array is explained in Appendix A. This has been done to further simulate the propagating effect for wind along the array. A concise schematic overview of the two-step analysis is given in Figure 5

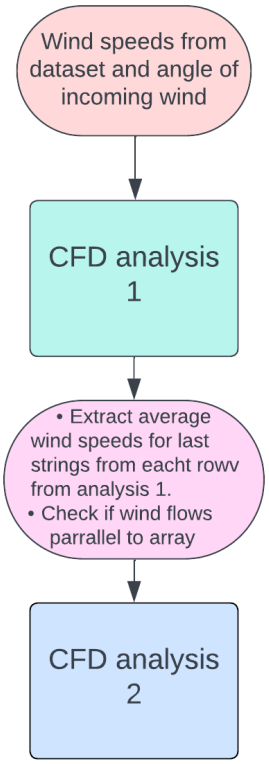

Figure 5: Schematic overview of the two-step analysis with inputs for each analysis

The results of the CFD analysis have been used to visualize the dynamics of the wind speeds underneath the array and how wind speeds develop when they advance underneath the array. The additional simulations have been used to create a contour plot showing the gradient of wind speed development at various heights and positions underneath the array. The contour

plot has eventually been used to determine a gradient for wind speed distribution underneath the array, which serves as input for the Python model to develop temperature dynamic data.

3.3 Establishing the thermal modelling

The thermodynamic model has been established following the proposed method of Rahaman et al. (2023). This model focuses on heat transfer from the incoming sun through the solar panel and out via the front and back sides of the array through convective and radiative heat transfer. The thermodynamic model has been established in Python using the Spyder programming environment.

For this thesis, only a part of Rahaman et al., 2023's method has been applied since the focus lies on the temperature dynamics between the array and the lake and not the heat loss through the front of the solar panels. Figure 6 on the left shows the considered layers in the proposed method. However, the method applied in this thesis project focuses on the heat transfer from zones two to three.

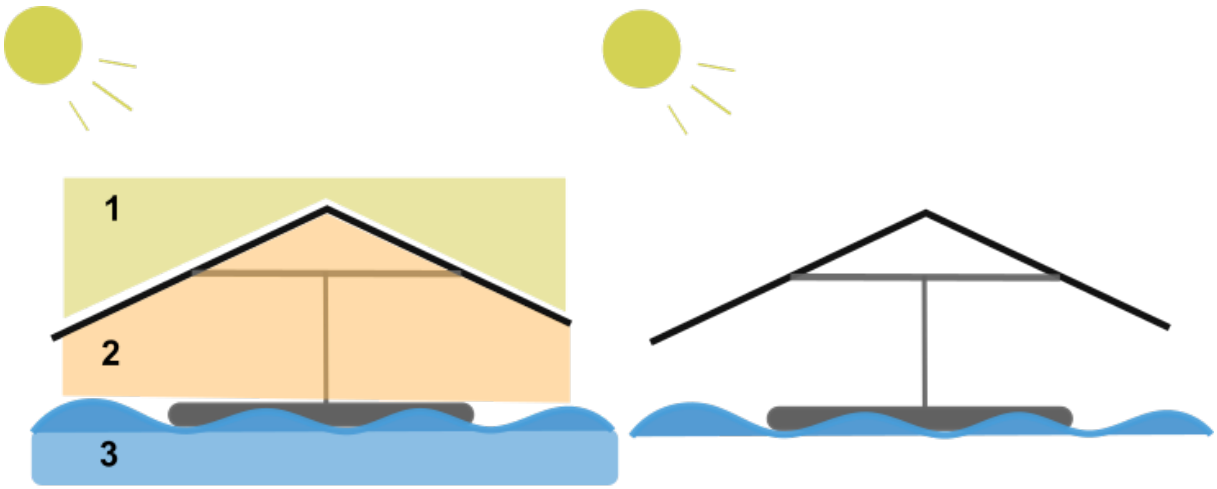

Figure 6: Basic representation of a floating solar panel and the targeted zones for modelling.

As the model required measurements that were not present in the dataset, approximations have been used to acquire the necessary data. To get an approximation for the water temperature equation (1) has been used in combination with the ambient temperature T_{amb} which is available through the Beilen dataset (Mackey and Berrie, 1991).

$$T_w = 4.29 + 0.55 \cdot T_{\text{amb}} \tag{1}$$

3.3.1 Heat input from the array

After approximating the missing data (more details are given in section section 4, first, the free and forced convection coefficients have been determined according to equations (2) and

(3)(Rahaman et al., 2023). The free and forced values have been determined for every time interval in the dataset.

$$Nu_{\text{free}} = f(Pr, Ra) \tag{2}$$

$$Nu_{\text{forced}} = f(Pr, Re) \tag{3}$$

The equations show how the Nusselt number is influenced by the Prandtl (Pr), Reynolds (Re) and Rayleigh(Ra) numbers, respectively (Rahaman et al., 2023).

Eventually, the free convective heat transfer for the backside of the solar panel is calculated with equations (4), (5) and (6) (Rahaman et al., 2023).

$$Nu_{\text{free}} = 0.15(Ra \cdot \cos\beta)^{1/4}; \text{if } 10^4 < Ra \cdot \cos\beta \leq 10^7 \text{ and } T \leq T_{\text{amb mod}} \tag{4}$$

$$Nu_{\text{free}} = 0.15(Ra \cdot \cos\beta)^{1/3}; \text{if } 10^7 < Ra \cdot \cos\beta \leq 10^{11} \text{ and } T \leq T_{\text{amb mod}} \tag{5}$$

$$Nu_{\text{free}} = 0.27(Ra \cdot \cos\beta)^{1/4}; \text{if } 10^5 \leq Ra \cdot \cos\beta \leq 10^{10} \text{ and } T > T_{\text{amb mod}} \tag{6}$$

Based on the result of the Nusselt values the free convective heat transfer coefficient for the back panel has been determined in (7) where K equals the thermal conductivity of air and L equals the area (in this case 1 m^2).

$$h_{c\ \text{free}}/h_{c\ \text{forced}} = \frac{Nu_{\text{free}}/Nu_{\text{forced}} \cdot K}{L} \tag{7}$$

To determine the Nusselt number for forced convection depending on the magnitude of the Reynold number (8) or (9) has been used (Rahaman et al., 2023).

$$Nu_{\text{forced}} = \frac{2 \cdot 0.3387 Re^{0.5} Pr^{1/3}}{\left(1 + \left(\frac{0.0468}{3}\right)^{2/3}\right)^{1/5}} \quad \text{if } Re \leq 5 \times 10^5 \tag{8}$$

$$Nu_{\text{forced}} = \frac{2 \cdot Pr^{1/3}}{1 + \left(\frac{0.037Re - 871}{5}\right)^{4/5}} \quad \text{if } Re > 5 \times 10^5 \tag{9}$$

For the forced convective heat transfer, the same equation as (7) has been used, albeit that Nu_free is substituted for Nu_forced.

$$h_{\text{cback}} = \sqrt[3]{h_{\text{cforced}}^3 + h_{\text{cfree}}^3} \tag{10}$$

The total amount of heat that gets moved from the back of the panel to the water is given by equation (11) (Rahaman et al., 2023).

$$Q_{\text{B conv}} = h_{\text{cb}} A (T_B - T_w) \tag{11}$$

Finally, to determine the radiative heat transfer from the back surface of the solar panels to the water equation (12) has been used. Here, ε refers to the emissivity of the back of the solar panel, φ refers to the view factor of the solar panel and the water surface, and σ is the Stefan-Boltzmann constant.

$$Q_{b_{\text{rad}}} = \varepsilon_{bw} \phi_{bw} A \sigma (T_w - T_B)^4 \tag{12}$$

Although Rahaman et al. (2023) mention in their paper that there is also conductive heat transfer from the back of the panel through the system's mounting to the water. It has not been used in this model as the contact surface is very small and heat transfer is assumed to be negligible. To get the total heat transfer for each iteration for various moments of the year, the code in Python iterates through the dataset, applying the relevant parameters in the equations to get the appropriate heat transfer for the given conditions. For each instance, then the sum of $Q_{\text{B conv}}$ and $Q_{\text{B rad}}$ represents the total heat transferred from the back of the solar panels to the water surface in W/m^2.

3.3.2 Net Heat Input (NHI)

The NHI is determined by adding the sum of incoming and outgoing heat flows of the lake; the heat flow is determined by equation (13). In addition, the lake has an incoming and outgoing flow, which can affect the temperature dynamics of the water by having an entering and exiting flow of warmer or colder waters. Due to the absence of data regarding the incoming and exiting flows regarding mass and temperature, the effect of the open system will be discussed qualitatively only.

$$H = (1 - \alpha) R_{sw} + (1 - \alpha) R_{lw} - H_{br} - H_c - H_e \tag{13}$$

R_{sw} represents the short wave irradiation, which has been measured by pyranometers present at Zonnepark Beilen.

R_{lw} refers to the incoming longwave irradiation and is calculated in equation (14) (Golroodbari and Sark, 2023).

$$R_{\text{lw}} = \varepsilon \sigma T^4 \tag{14}$$

H_{lw}, H_c and H_{le} represent the outgoing long wave radiation, sensible heat and latent heat, respectively.

These are calculated with the following equations (Golroodbari and Sark, 2023):

$$H_c = \rho_a c_p v_w \Delta T \tag{15}$$

$$H_e = \rho_a L_v v_w \Delta RH \tag{16}$$

ρ_a refers to the air density, v_w refers to the wind speeds at the water level. c_p is the specific heat capacity of air, L_v is the latent heat of vaporization. ΔRH is the difference between the relative humidity of water and air, where the relative humidity for water is always 1 (Golroodbari and Sark, 2023).

$$H_{br} = \varepsilon_{ws} \sigma (T_{ws})^4 \tag{17}$$

For equation (17) ε_{ws} refers to the emissivity of the water surface, which in this case has been given the value of 0.85. σ once again is the Stefan-Boltzmann constant and T_{ws} is the temperature of the water surface(Golroodbari and Sark, 2023).

With both the NHI and array heat input modelled in a Python script, the dataset acquired from Zonnepark Beilen can be used as input data. Eventually, a years' worth of data from 01/01/2022 - 01/01/2023 will be used for computing the results, as this year proved to be the most complete, with little gaps that had to be filled with interpolation.

3.4 Economic assessment

Due to time limitations, the economic assessment follows the thermodynamic and environmental impact analysis and has been limited to a qualitative approach. For the economic assessment, research has been done on how the environmental impacts translate to opportunities or risks for economic activities like fish cultivation/harvesting. The results have been put into perspective focusing on how the added potential for economic activities can benefit FPV systems in economic terms like offsetting Capital Expenditures (CAPEX).

4 Data Analysis

Zonnepark Beilen is situated in the Drenthe province, located in the middle-north of the Netherlands. The FPV system is installed on a lake primarily used for winning sand. The water body itself has an entering and exiting flow of water located near the south; a satellite image of the 9.6 ha FPV system in Beilen is shown in Figure 7.

Figure 7: Aerial view of Zonnepark Beilen

The array has panels facing east and west with a 12° angle from the horizontal and ± 90° azimuth angle featuring 400 and 405 Wp solar panels (39,256 panels in total) covering roughly 50% of the lake's surface (Cooperatie Project de Mussels, 2023). The output of the solar panels is converted to AC power by 182 converters, bringing the nominal AC output to 10.92 MW. Further dimensions from a cross-section of the solar array can be seen in Figure 8.

4.1 Dataset overview

The acquired dataset from Zonnepark Beilen features roughly two years' worth of data (22-04-21/06-09-23). The dataset features information regarding the total output of the FPV system and features measurements from three measurement points present in the system. The data

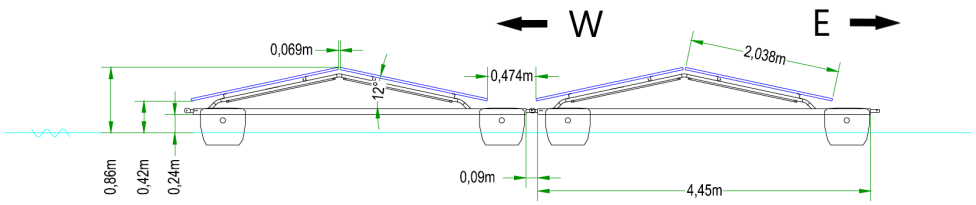

Figure 8: Dimensions, orientation, and tilt angle of the solar panels in the array (GroenLeven, n.d.).

set proved to be relatively clean of data errors. On several occasions, the wind speed measured for area one registered errors in both wind speed and wind direction. The values were equally high for both the wind speed and wind direction, reaching unrealistic numbers (200 km/h wind speeds). This indicates a sensor or data error, probably resulting in the maximum sensor value being stored. These data points have been treated as missing values and were given the NaN flag in the data set to be handled later during interpolation steps.

The weather station at location '7' reported false information for five consecutive days (1-10-21/6-10-21). The parameters of Solar irradiation (east and west), wind speed, and wind direction were determined to be false due to unrealistic high wind speeds, unreasonable wind speed directions (values higher than 360), and the presence of the same amount of solar irradiance through the day and night. The data from location 1 appears to be intact. After conducting statistical tests of neighboring data, data between the two weather stations (when functioning correctly) showed no significant differences.

4.2 Missing data

The acquired data has some missing values for every parameter; the amount of missing measurements for each parameter and the measures taken to correct these in the data set can be seen in Table 1. For the missing output data, no interpolation has been used as all missing values (8) occurred during the night when no solar irradiation was present. Therefore, the output has been determined to be 0 for all missing data points. Filling in missing values for solar irradiance is done by linear interpolation, as linear interpolation, when accompanied by sufficient neighbouring data points, is well suited to fill in missing irradiance data (Denhard et al., 2021). For interpolating the ambient temperature at the site location Baltazar and Claridge (2006) mention that in comparison to spline-based and Fourier-based interpolation techniques, linear interpolation is deemed to be superior for filling gaps in data sets.

4.3 Wind speed and wind direction

The array provides useful parameters that will serve as inputs for the Python model as they are. However, the wind speeds and wind direction are important metrics for the CFD analysis.

Table 1: Missing data from Beilen dataset

Parameter	**No. of Missing values**	**% of total**	**Interpolation type**
AC Output	8	0.01%	None
KBN Beilen T01-P-et-1 [W/m^2] Irradiation East facing panels	16	0.01%	Linear
KBN Beilen T01-P-wt-1 [W/m^2] Irradiation West facing panels	16	0.01%	Linear
KBN Beilen T01-Ta-p-ts [°C] Ambient temperature	19	0.02%	Linear
KBN Beilen T01-Wd-p-ts [°] Wind direction	16	0.02%	Moving average
KBN Beilen T01-Ws-p-ts [m/s] Windspeed	16	0.02%	Moving average
KBN Beilen T03-Tm-t-et-1 [°C] Module temperature East facing Panels	9	0.00%	Linear
KBN Beilen T03-Tm-t-wt-1 [°C] Module temperature W-facing Panels	9	0.00%	Linear
KBN Beilen T07-P-et-1 [W/m^2] Irradiation E-facing panels	8	0.01%	Linear
KBN Beilen T07-P-wt-1 [W/m^2] Irradiation W-facing panels	8	0.01%	Linear
KBN Beilen T07-Wd-p-ts [°] Wind direction	8	0.01%	Moving average
KBN Beilen T07-Ws-p-ts [m/s] Windspeed	8	0.01%	Moving average

The measured wind speeds do not represent the same dynamics as below the array. To make an accurate setup for the CFD analysis the main wind speed and direction have been extracted from the data and visualized in Figure 9.

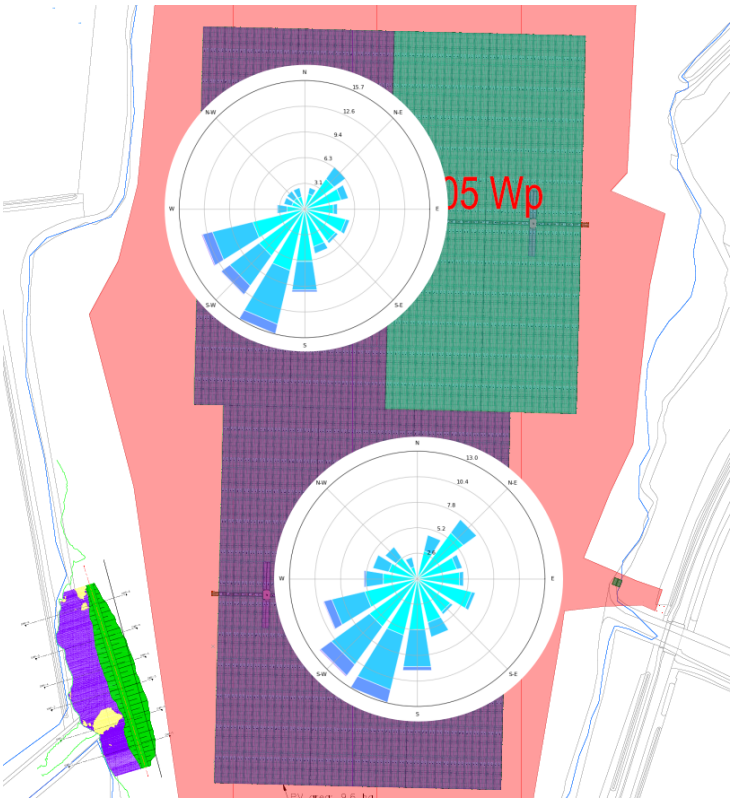

Figure 9: Most occurring wind speeds and directions measured at Zonnepark Beilen. The windroses in the figure are placed based on the locations of the weather stations present on the array.

4.4 Relative humidity

Relative humidity is an important parameter to determine heat loss by evaporation and is required to calculate the NHI. As the data for relative humidity at Zonnepark Beilen was not present in the dataset, the data has been acquired from NASA weather databases, which compute various weather variables through satellite imagery (NASA, 2023a). The data available for relative humidity at the location of Zonnepark Beilen was available for the year 2021 until 2023 at intervals of one hour. The dataset contained no gaps.

5 Results of the CFD Analysis

5.1 3D modelling and CFD setup

A 3D input model for the CFD analysis has been created in the Autodesk Fusion 360 software. Due to constraints in computational power, several iterations of Zonnepark Beilen have been constructed. One model at full size and scale, one single string of 18 panels for model testing purposes and one 20-string variant compliant with the maximum available computational power.

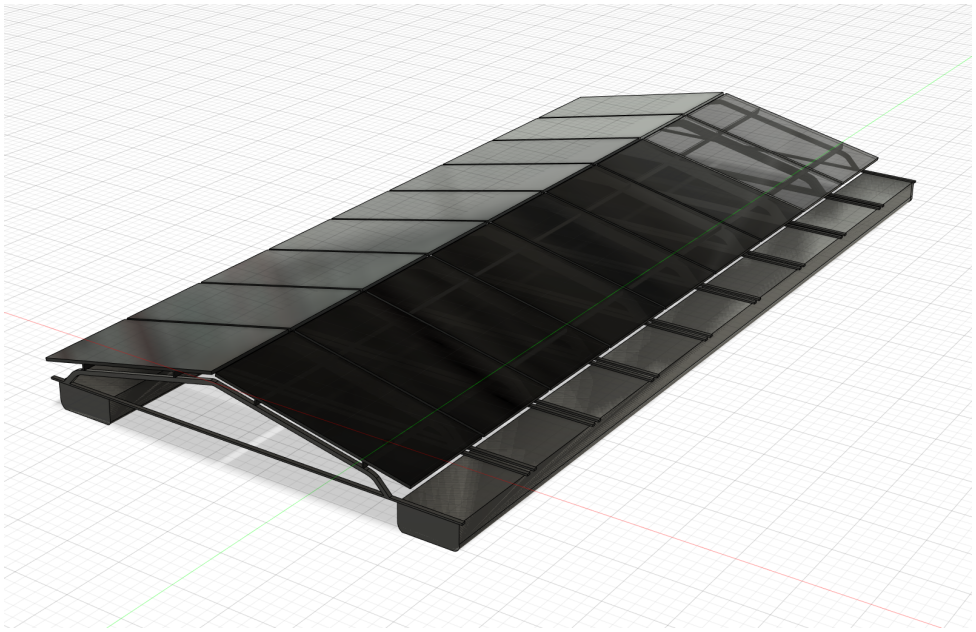

Figure 10: Digital render of one string composing the FPV system at Beilen

The constructed 3D models have been exported as .step files to Autodesk CFD software for further CFD processing. The model setup consisted of assigning material properties to the strings like aluminum struts, glass solar panels, and plastic floaters. Afterwards, a new volume has been created surrounding the 3D model which has been assigned as a variable air volume with a starting temperature of 20°C (Figure 11). The angle for approaching wind has been determined from the data analysis results and resulted in a 30° angle. The initial solver parameters have been set for a non-compressible fluid with a developed air inlet profile. Choosing these settings will result in the most accurate results when considering a natural environment. The second analysis has been set up with the same parameters except for the angle of the incoming wind which in this case has been reduced to 0. The solver has been set to run for 500 iterations or to stop when convergence has been achieved. For extracting wind velocity data different layers of measurements have been chosen as the air underneath the array moves at different speeds for different heights.

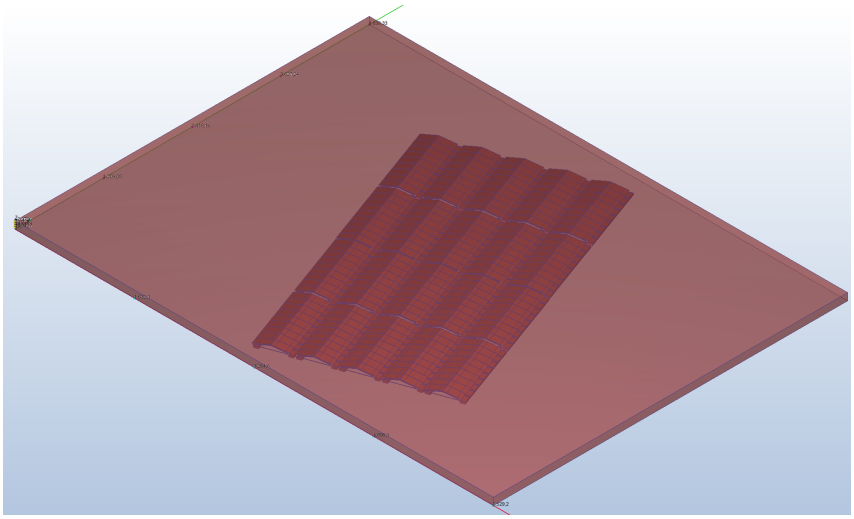

Figure 11: Composed model of a 20-string array including an assigned fluid (air) on all surfaces indicated by the red box.

5.2 Planar analysis and velocity magnitudes

This section contains results from the CFD analysis. The results have been established by extracting measurements from cross-sectional planes through the simulated airbox.

5.2.1 Wind dynamics at water and rack mounting level

For the analysis of the CFD results different sections of the FPV array have been chosen to gather wind speed data. These are the water surface level, the mounting system level (referred to as rack level later on), and the west and east-facing layers right below the solar panels. These sections have been chosen as these layers represent the wind speeds related to the convective heat transfer between the solar panels and the water surface. Figure 12 shows the constructed planes used for the water and rack height analysis of the two CFD analyses that have been executed. In Figure 12a and Figure 12b the wind speed distribution underneath the array has been visualized. For the edges facing the incoming wind (row 1, string 1-4) the wind speeds are the highest while afterward gradually declining throughout rows 2-5. With the lowest wind speeds being simulated at row 5 string 4. Another effect that can be noticed is that the wind speed at the water level is in general higher than at the rack level (also noted in Table 2). The effect is likely caused by a cushioning effect as air can enter the array at rack height creating an interrupting flow and interrupting the air from progressing higher up. The increased airflow across the water surface therefore only has an effect for the first 24 centimeters from the water surface before it starts to lose its effect.

The dynamic of the wind losing its energy while progressing through the array is also notable in Figure 12c and Figure 12d where the decline in wind speed is also visible albeit less clear due to the decreasing rate of energy loss by the wind. The effect of wind losing its energy while passing the array is also highlighted by the wake of slow air present in Figure 12a and Figure 12b that would otherwise be other strings of solar panels weren't it for the computational limitations

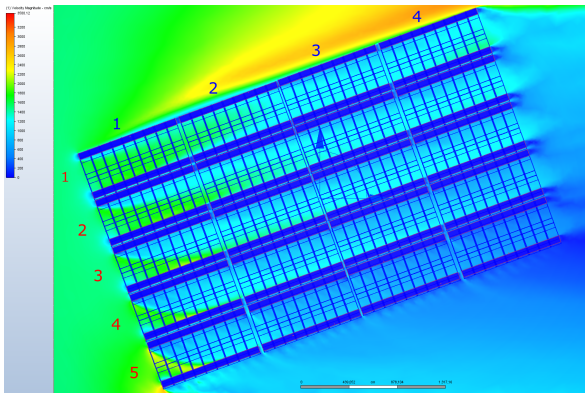

(a) Analysis 1 water level

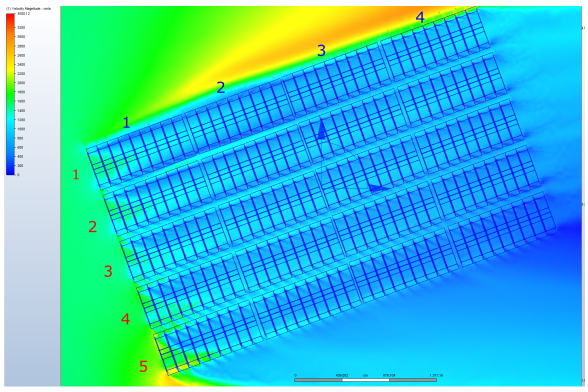

(b) Analysis 1 rack level

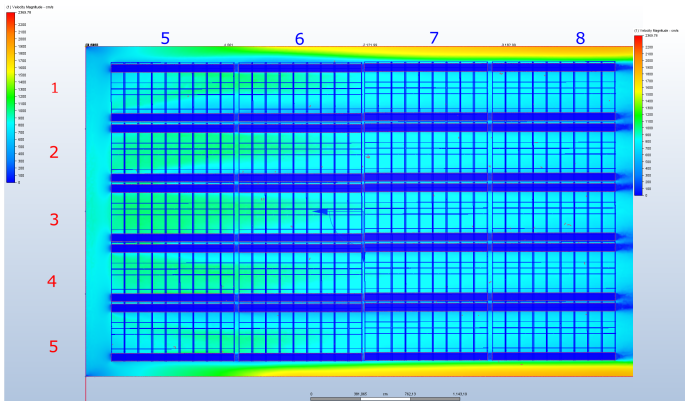

(c) Analysis 2 water level

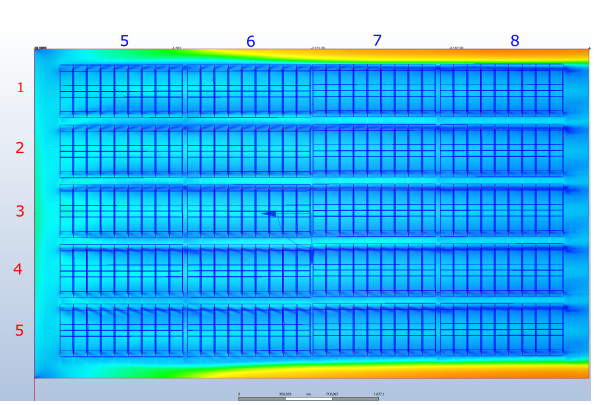

(d) Analysis 2 rack level

Figure 12: Analysis 1 and 2 featuring the wind speeds at water and rack level height. The rows are indicated in red and the strings in blue respectively.

of this project. The orange wakes present in Figure 12a and Figure 12b are occurring across the length of the array as the incoming wind collides with the array and is redirected along the strings. For Figure 12c and Figure 12d the increased wind speeds would only occur if the panels happen to be on the outer west side of the array (in the case of Zonnepark Beilen).

Next to the visualization of the wind speed dynamics, quantitative data has also been extracted from the model. The data is represented in Table 2 for both the water and rack level heights. As mentioned before it can be seen that the wind speeds at rack level are generally lower for each string compared to the water level. The 'sudden' increase in wind speeds occurring from string 5 in rows 3-5 comes from a limitation in the simulation. The second analysis had to be run with an initial wind speed that has been set as the average wind speed at the exit of the array from all rows in the first analysis. This resulted in an average that is on some occasions higher than the existing wind speed. Additionally, the behavior of wind in the first analysis is different to the second analysis as the wind is coming in from an angle. These different dynamics can be seen by the way the colors change with the values in Table 2. The effect is shown in Figure 12a and Figure 12b with higher incoming wind speeds at row 1 string 1 and lower exiting wind speeds after the array at row 5 string 4 are also reflected by the numerical data. The second analysis shows a more gradual decline along the strings across all rows.

Table 2: Weighted averages of the velocity magnitudes per string at water and rack level heights. Wind speeds are given in m/s

water level						Rack level					
String	Row					String	Row				
	1	2	3	4	5		1	2	3	4	5
1	15.38	14.41	12.87	11.49	11.08	1	11.16	11.1	10.63	10.5	10.67
2	13.2	11.74	10.73	9.2	7.03	2	8.03	8.1	8.02	7.62	6.65
3	10.39	10.38	9.51	7.93	5.42	3	7.01	7.47	7.28	6.45	5.09
4	11.15	10.39	9.32	7.35	4.48	4	8.34	7.59	6.89	5.6	3.788
5	8.12	9.05	8.48	6.45	5.12	5	6.36	6.74	6.89	6.65	3.8
6	7.7	8.25	7.46	5.33	4.9	6	5.48	5.56	5.61	5.29	3.2
7	7.13	7.46	6.45	5.21	4.55	7	4.84	5.05	5.02	4.92	3
8	7.16	7.22	6.23	5.01	4.41	8	4.81	4.85	4.85	4.76	3.1

5.2.2 Wind dynamics directly underneath the solar panels

Additional to the data gathered on the water and rack level wind speed dynamics have also been visualized right beneath the solar panels. This gives valuable information regarding how the wind behaves at this part of the array and will help to more accurately determine the convective heat transfer from the back of the panels.

In Figure 13 the wind speed distribution underneath the solar panels is visualized. Compared to the dynamics on rack and water level of the array the wind speeds underneath the solar panels are in general slower in both east-and west-facing directions. In addition to the lower wind speeds the variations in wind speeds across the array are also less noticeable compared to the water and rack level. One notable dynamic is the increased wind speed that the first strings are experiencing in rows 4 and 5 compared to the first rows. In the first simulation (Figure 13a and Figure 13c), the distance for the air to get to the array is longer for rows 4 and 5 compared to row 1. This means that in the simulation the wind has a larger area to cover before entering the array. The increased area results in more air mass and larger incoming air pressure at the beginning of the array, generating a wind speed increase as the air pressure reduces when being forced down a smaller pathway. Another insight given by these figures is that the wind speeds underneath the solar panels are less susceptible to wind coming in from the sides of the array. This indicates that the wind speeds directly underneath the solar panels are more stable and consistent throughout the array.

The weighted averages of the velocity magnitudes for each string are represented in Table 3. The same phenomenon with the wind speed increasing from row 5 string 4 to row 5 string 5 is also explained by the starting parameters of the second analysis. The wind speeds underneath the solar panels show a more gradual decline due to less interference from wind coming from the sides.

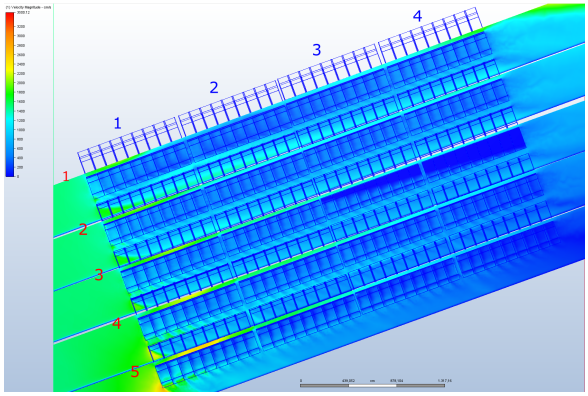

(a) Analysis 1 East facing panels

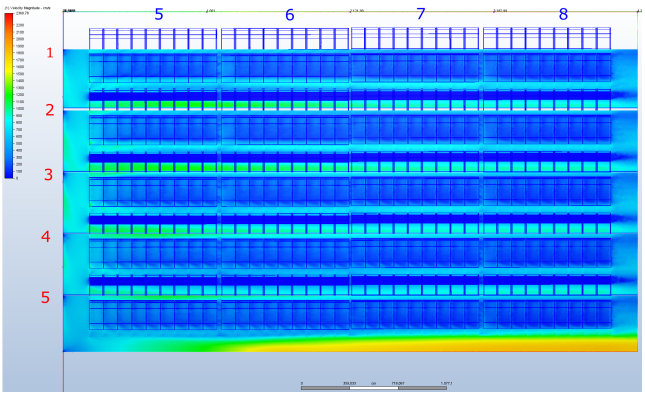

(b) Analysis 2 East facing panels

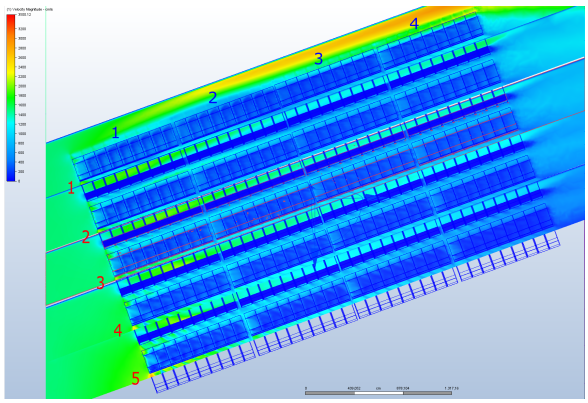

(c) Analysis 1 West facing panels

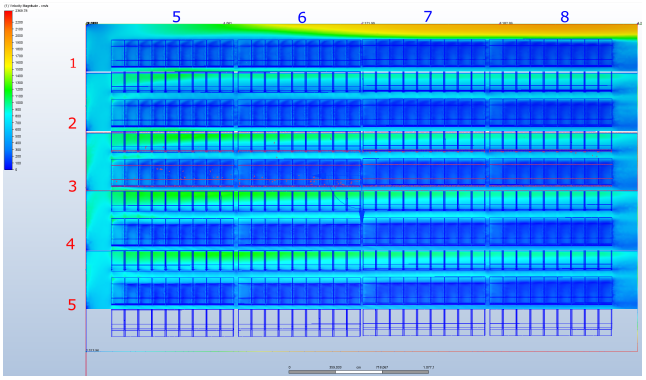

(d) Analysis 2 West facing panels

Figure 13: Analysis 1 and 2 featuring the wind speeds just below the east and west-facing solar panels. The rows are indicated in red and the strings in blue respectively.

Table 3: Weighted averages of the wind speeds just below the solar panels in the array. Wind speeds are given in m/s

water level						Rack level					
String	Row					String	Row				
	1	2	3	4	5		1	2	3	4	5
1	4.47	4.77	4.73	4.9	4.01	1	4.97	5.08	6.1	5.93	6.92
2	3.07	4.16	3.86	3.86	3.4	2	3.32	3.71	4.2	4.23	4.38
3	3.9	3.69	3.65	3.21	2.85	3	3.36	3.6	3.55	3.37	3.02
4	3.3	4.1	3.72	3.13	2.28	4	4	3.6	2.59	2.65	1.74
5	2.53	2.55	2.74	2.9	2.9	5	2.97	3	3.13	3.16	2.8
6	2.03	1.77	1.95	2.22	2.46	6	2.46	2.17	2.11	2.28	2.24
7	1.78	1.76	1.92	1.95	2.21	7	1.97	1.88	1.89	1.92	1.75
8	2.05	1.89	1.83	1.91	1.9	8	1.71	1.9	1.87	1.91	1.8

5.2.3 Trend lines and application for the entire array

The results from the CFD represent how the wind speed dynamics are likely to behave at important points underneath a section of the array in Beilen. However, the simulated sample is too small to assume that the wind speeds are the same for the entire array. Therefore, trend lines from the generated data have been established for different sections of the array. These trend lines will be used in the Python model to generate wind speeds that are more fitting for the location of the strings in the array rather than to assume one value for the entire array. Multiple trend lines have been established to represent different parts of the array that experience different dynamics.

The strings facing the incoming wind and the edges of the system on the west side of the array have been assigned to the trend line generated from the part 1 analysis. This holds for the water surface wind speeds, as well as both the east and west-facing panel wind speeds. The other strings in the array that are not directly facing the incoming wind and trend lines derived from the second analysis will be applied for the same measurement levels. Because the trend lines are based on simulations containing 4 strings per row, the entire array has been subdivided into 11 zones, each featuring 4 strings. Additionally, the large blue zone in Figure 14 represents the wind-facing panels, which will be seen as one area. For each zone, the distance underneath the array will be updated into the derived trend line equations, resulting in wind speeds tailored to the position of strings underneath the array. The subdivision of Zonnepark Beilen into segments can be seen in Figure 14.

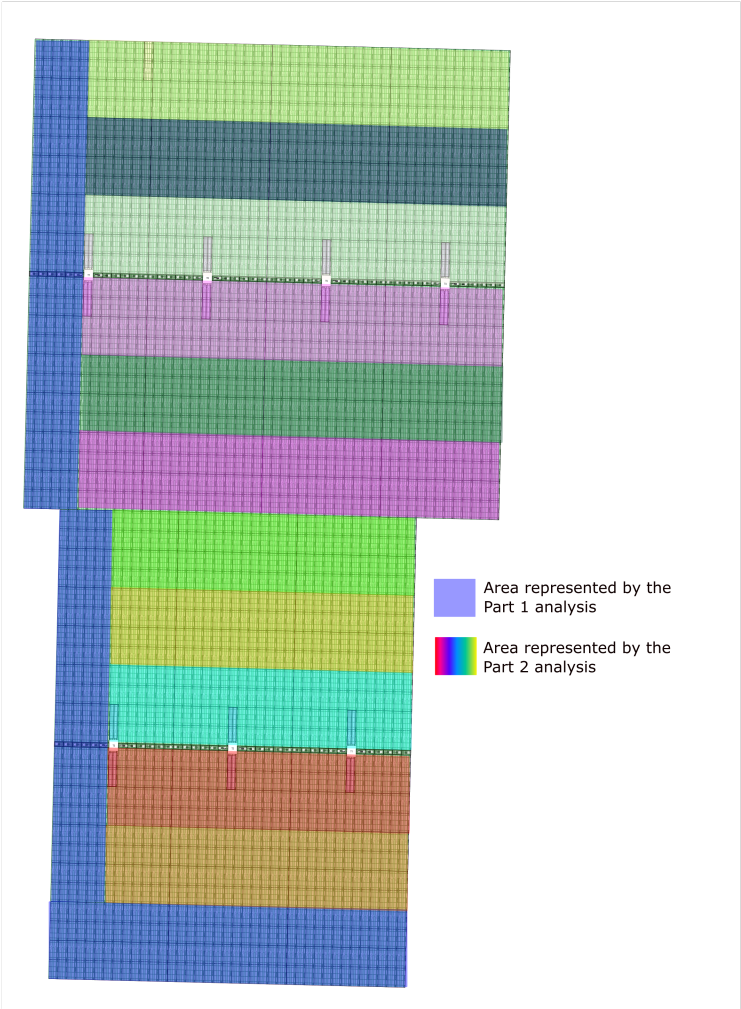

Figure 14: Division of the zonnepark Beilen array into zones for adjusted wind speeds. Note the difference made for strings facing south and west compared to strings not directly facing the incoming wind.

The trend lines derived from part 1 for the east and west-facing panels are highlighted in equations (18) and (19). For the wind speeds at the water level, equation (20) has been used. Variable x represents the string number in the array from where the wind enters the respective zone. As each zone has a length of 4 strings, calculating the wind speeds in the second zone (orange color from the bottom of Figure 14) would mean that a value of 4 is assigned for variable x.

$$V_{\text{wind\_east\_1}} = 6.8 \cdot e^{-0.22x} \tag{18}$$

$$V_{\text{wind\_west\_1}} = 9.3 \cdot e^{-0.06x} \tag{19}$$

$$V_{\text{wind\_water\_1}} = 14.4 \cdot e^{-0.15x} \tag{20}$$

For the the rows of strings that do not face the incoming wind directly and experience wind dynamics parallel to the array direction the following set of equations has been used:

$$V_{\text{wind\_east\_2}} = 3.334 \cdot e^{-0.166x} \tag{21}$$

$$V_{\text{wind\_west\_2}} = 2.842 \cdot e^{-0.114x} \tag{22}$$

$$V_{\text{wind\_water\_2}} = 9.256 \cdot e^{-0.069x} \tag{23}$$

The equation (21) will apply to the east-facing panels, equation (22) will apply to the west-facing panels, and (23) is applied to the wind speeds at water level. The exponential equations have been established by applying an exponential curve to the values extracted from the CFD model, which shows that wind speeds decline more rapidly just before they enter the array but the decline slows gradually when progressing further. Using a linear relation could possibly fit wind speed reduction even when looking further underneath the array but due to modelling restraints, this could not be determined.

6 Thermodynamic modeling results

With the equations established from the data generated by the CFD model, the thermodynamic model has been run. In total, 13 sets of data have been generated, each set represents a zone as highlighted in Figure 14. The output of the model indicates the heat transfer from the FPV system to the water. In addition to the heat input from the array to the water, the NHI shows the heating dynamics based on the same data from Zonnepark Beilen but highlights the heating effect as if the FPV system is not present.

6.1 NHI and array heat input

The NHI and array heat input data have been generated as mentioned in section 3.3 with the addition of the established wind speed equation from section 5.2.3. The output data has been generated by applying the equations for sub-panel wind speeds and wind speeds across the water surface in the model where these values were required. Due to the nature of the equations, a gradual decline in wind speed (and therefore energy in the wind) has been noted as the wind progresses through the length of the array. An overview of the heat transfer dynamics for the array is given in Figure 15. The figure highlights three dynamics, the NHI, the heat input from zone 1, and the heat input from zone 12. Highlighting zone 1 and 12 shows the difference between the upwind side of the array compared to the downwind side of the array.

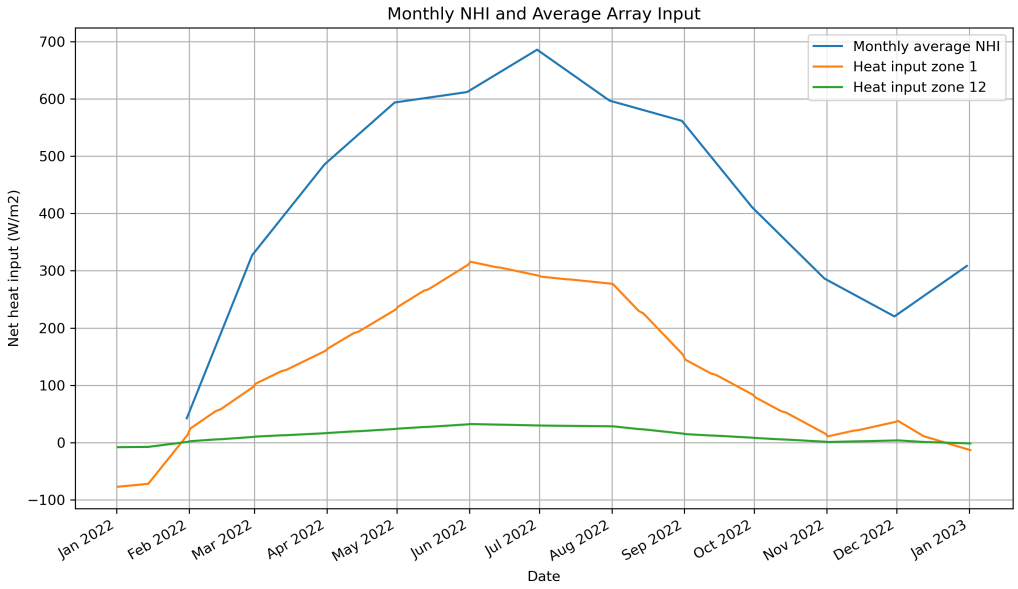

Figure 15: Visual representation of the NHI and array heat input throughout the year. Array zone 1 and zone 12 represent the first and last row in the array. (Note that the monthly average NHI starts at the end of January due to Monthly sampling on the last day of the month.)

It can be seen in Figure 15 that zone 1 and 12 do not exceed the NHI throughout the year. indicating that per m^2 more energy in the form of heat is entering the lake when the array is not present. This is especially the case for zone 12, where the NHI is relatively steady throughout the year and near zero. In this figure, the negative part of the graph for zones 1 and 12 indicates that the lake is losing its energy towards the array, indicating that the lake is cooling down in the upper water layer. Throughout the year the reduction in global NHI and the heat input from the array in zone 1 differs between 144% and 45% (Table 4). The percentages $> 100\%$ mean that the heat flow is reversed and thus the lake is cooling down.

Table 4: Summarized data for the year 2022 including the difference in NHI for zones 1 and 12.

Month	avg. NHI (W/m2)	avg. NHI form zone 1 (W/m2)	ΔNHI	$\Delta\%$	avg. NHI from zone 12 (W/m2)	ΔNHI	$\Delta\%$
Jan/22	174.82	-76.96	-251.79	-144%	-7.93	-182.76	-105%
Feb/22	348.13	24.58	-323.54	-93%	2.49	-345.63	-99%
Mar/22	337.71	102.89	-234.82	-70%	10.54	-327.17	-97%
Apr/22	502.11	164.46	-337.64	-67%	16.90	-485.21	-97%
May/22	594.16	237.31	-356.85	-60%	24.40	-569.75	-96%
Jun/22	578.80	315.69	-263.10	-45%	32.46	-546.33	-94%
Jul/22	703.93	289.77	-414.15	-59%	29.82	-674.10	-96%
Aug/22	623.28	276.62	-346.66	-56%	28.46	-594.82	-95%
Sep/22	564.15	144.70	-419.45	-74%	14.87	-549.27	-97%
Oct/22	472.10	78.95	-393.14	-83%	8.12	-463.98	-98%
Nov/22	294.88	10.96	-283.91	-96%	1.11	-293.76	-100%
Dec/22	296.64	38.05	-258.59	-87%	3.95	-292.68	-99%
Jan/23	218.51	-13.06	-231.58	-106%	-1.34	-219.85	-101%

Because the wind speeds underneath the solar panels and at the water surface differ greatly depending on the location of the array a contour plot has been made. The contour plot shows where on the array more energy is transferred from the array towards the water surface (or the other way around). The dynamics are shown per season to give additional insights into how these dynamics change throughout the year. The contour plots for the four seasons are shown in Figure 16. The contour plots show how the heat input from the array to the water is highest at the edges facing the incoming wind and then gradually declines towards the top right of the array. These dynamics take place throughout the year except for fall (Figure 16c) where the gradient is not apparent. The low gradient during fall is due to the, on average small decline in temperature throughout the season and the small difference between module and ambient temperature. The lower temperature delta results in a slower decline in heat transfer as the wind loses energy.

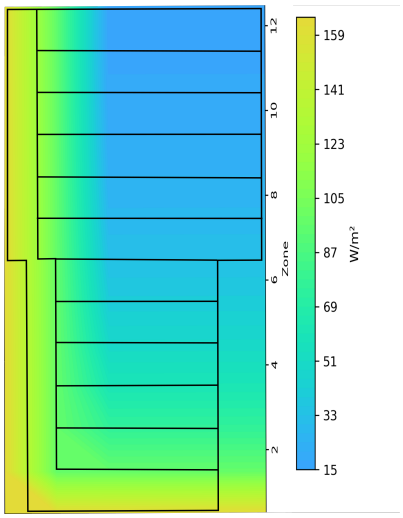

(a) Heatflow distribution of the array during spring

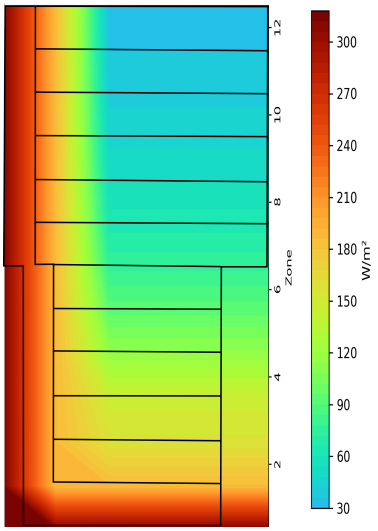

(b) Heatflow distribution of the array during summer

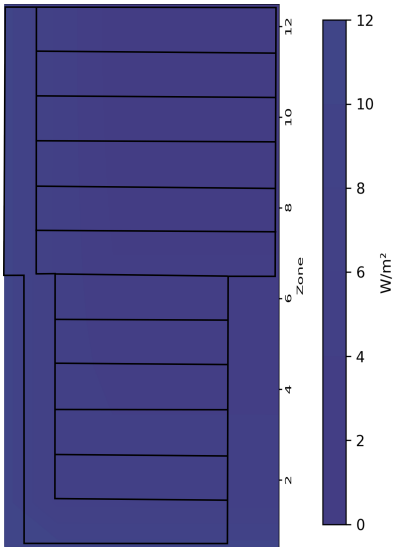

(c) Heatflow distribution of the array during fall

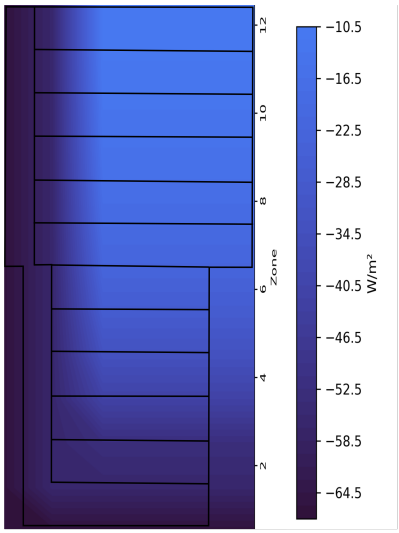

(d) Heatflow distribution of the array during winter

Figure 16: Four contour plots overlapped on the graphical layout of Zonnepark Beilen, highlighting the distribution of heat input to the water.

6.2 Module temperature and uncertainties

In the field of FPV the U-value is used to determine the ability of a solar module to lose accumulated heat by incoming irradiation to the environment. Dörenkämper et al. (2022) write the following expression for the U-value in (24).

$$U = \frac{\alpha \cdot G_{\text{POA}} \cdot (1 - \eta)}{(T_{\text{mod}} - T_{\text{amb}})} \tag{24}$$

Where α is the fraction of the absorbed solar spectrum, G_{POA} the in-plane irradiance and η the module conversion efficiency. U is expressed in W/m^2K and can be decomposed in a constant part, and wind speed dependent part see equation (25).

$$U = U_C + \nu \cdot U_\nu \tag{25}$$

Where ν is the wind speed at module height. A higher U-value means that a module is able to lose more heat to its environment. Equation (24) and (25) show how the ability of solar panels to lose heat to their environment is dependent on the portion of absorbed irradiation and the difference between the module temperature and the ambient temperature.

The regression trends for the relation between the U value and wind speeds have been established for irradiation and temperature of two locations on the array. The scatter plot and accompanying regression are shown in Figure 17, Figure 18, Figure 19, and Figure 20.

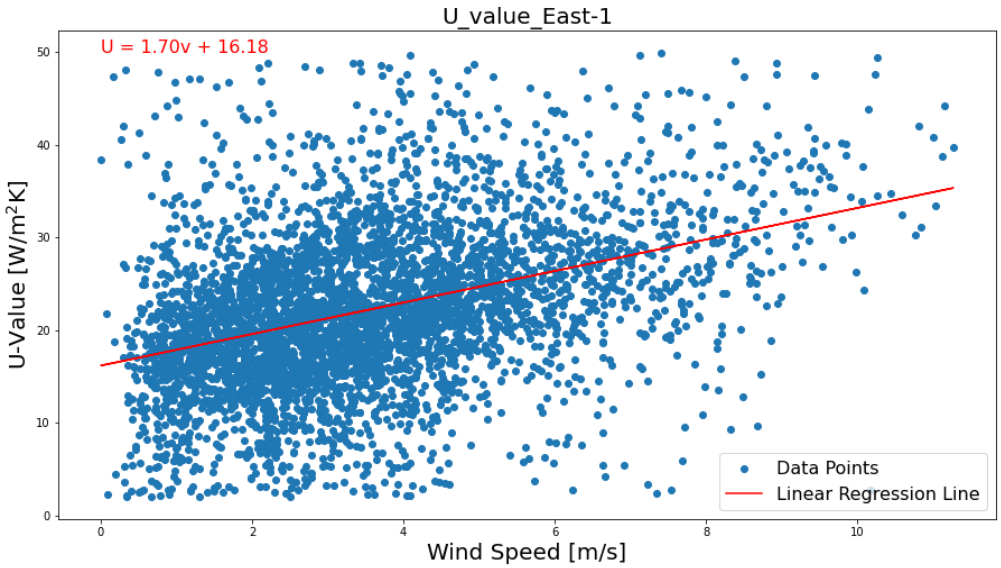

Figure 17: Regression east-facing panels on location 1

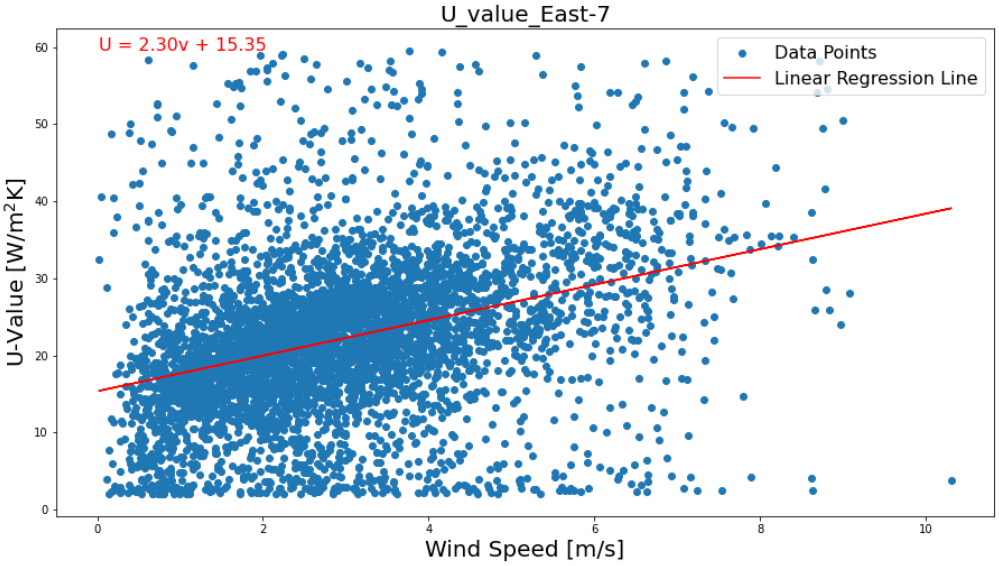

Figure 18: Regression east-facing panels on location 7

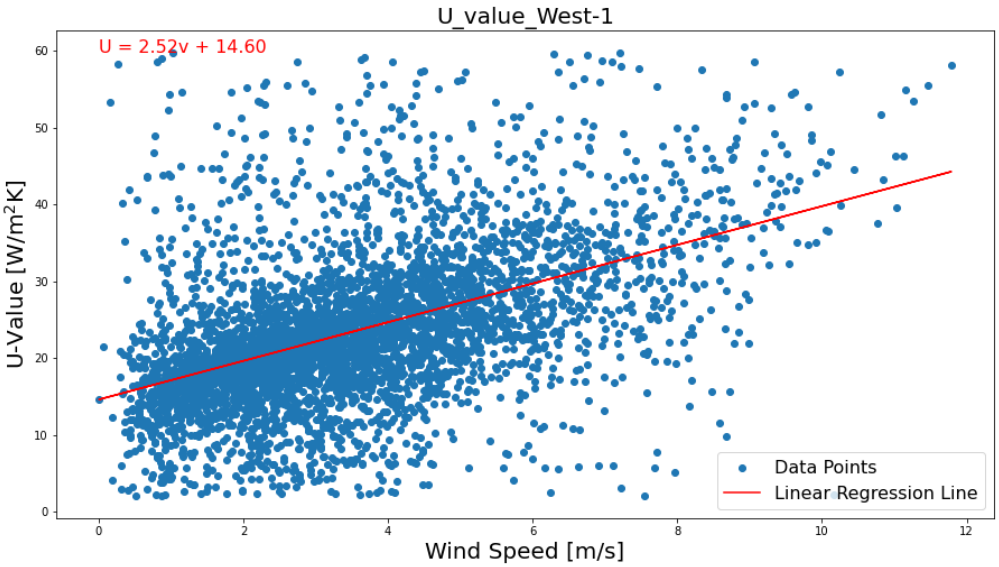

Figure 19: Regression west-facing panels on location 1

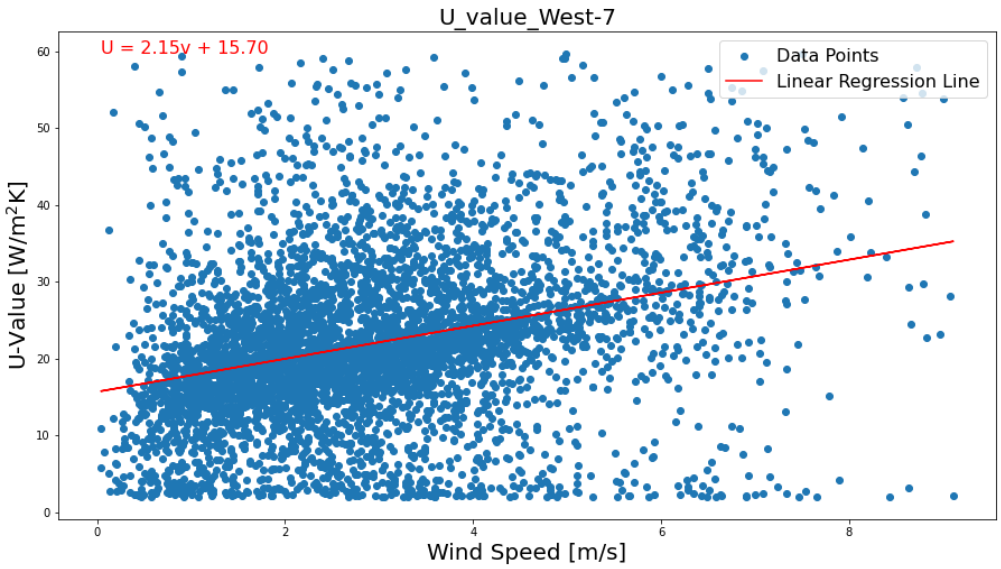

Figure 20: Regression west-facing panels on location 7

The figures feature data points from measurements throughout the year based on irradiation temperature and wind speed data, highlighting the positive linear relationship between wind speed and the U value. Rewriting equation (24) by combining it with equation (25) and substituting ν with equations (18), (19), (21), and (22) allows us to determine the U_v-value based in the x value. This means that, for this array, the U_v-value can be determined for any spot on the array by inserting the distance that the wind has traveled underneath the array for value x (starting from the south).

$$U_v = \frac{\frac{\alpha \cdot G_{POA} \cdot (1-\eta)}{(T_{mod} - T_{amb})}}{a \cdot e^{-bx}} - U_c \tag{26}$$

In equation (26) a and b are the terms used for wind speeds underneath the east and west-facing panels for both steps one and two of the CFD analysis.

Additionally, the wind speed is an important multiplier for the amount of heat that can be transferred to the environment. In the acquired dataset from Zonnepark Beilen, the module temperatures for only one place in the array were measured. Therefore, all temperature differences between the module and ambient temperature would be the same throughout the array. However, the U-value shows how solar panels lose their ability to transfer heat when module temperature is increased or when wind speeds are lower. While the model accounts for decreased wind speeds along the array, it is expected that modules on the north side of the array lose less heat compared to those on the south side. This results in warmer module temperatures, and therefore lower panel efficiencies (see Figure 1). Therefore it is likely that power generation by the array is not uniformly distributed across all strings. Looking at the contour plots in Figure 16 it is likely that the zones with lower heat transfer to the water are the same zones that produce less power as a result of warmer modules and lower conversion

efficiencies.

6.3 Impact on water temperature

While the solar array releases some of the absorbed energy back to the water surface in the form of heat, there is notably less heat entering the water surface compared to when the array would not be present. To determine the impact that the reduced irradiation has on the water surface temperature, the difference in incoming irradiation from the sun and the array has been calculated. It is assumed that the water temperature as-is is based on the fact that no coverage is applied over the water surface. As mentioned in section 3.3 the water temperature is approximated with equation (1). Albeit the approximate water temperature might not be reflective of the actual water temperatures and is likely lower than the actual, the effect of reduced irradiance will still provide usable insights about surface temperature reduction. The temperature reduction caused by the reduced NHI is done for the surface water level which has been arbitrarily set to a depth of one meter. Therefore, the reduced temperature of the water surface level will be expressed in $^{\circ}C/m^3$. The results are shown in Figure 21.

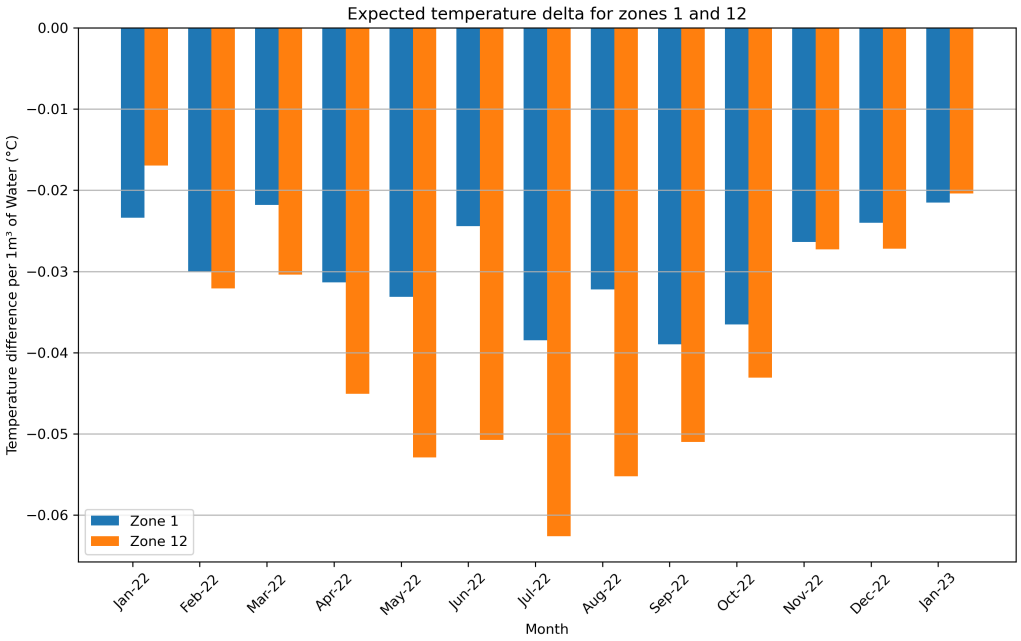

Figure 21: The suspected temperature differences for the water surface for each month, based on the reduction in NHI.

As expected from the previous insights in Table 4, the water lying underneath the array in zone 12 receives notably less heat from the solar panels. The second component of equation (25) will be nearly zero for zone 12 as wind speeds have dropped notably in that place of the array. As a result, solar modules in zone 12 may have a higher back sheet temperature. For zone 1 the water receives more heat from the back sheets of the solar modules as the U-value is higher due to higher wind speeds. Therefore, the water surface is experiencing a larger cooldown effect in zone 12 compared to zone 1 (Figure 21). It is noteworthy that the total

cooled volume is restricted to 1 m^3 which is not the case in the real world, where seasonal variations play a large role. For example, Heiskanen et al. (2015)., mention that due to the higher temperatures in spring, the water surface loses more heat due to increased turbulent flows of sensible and latent heat mixing the water with colder, lower layers of the lake. In the fall, this effect is lower due to decreased lake temperature and overall temperature changes. Because of this effect, the trend in Figure 21 should not be seen as absolute cooling but rather as the cooling potential for the water surface. The mixing effect distributes the heat throughout the lake but also has the side effect of distributing nutrients and oxygen among the lake. The lower surface water temperatures on the water surface combined with the lower wind speeds across the water surface underneath the array (mainly at the downwind side) can significantly reduce thermal stratification. Reducing said distribution of water nutrients and oxygen, which in turn has negative effects on marine life (Obbink, 2023). Because the wind speed and temperature dynamics on the water surface are not uniform across the area underneath the array, impacts are also likely to vary. With the contour plots from Figure 16 in mind, the impact of reduced wind speeds and reduced temperatures will likely increase when progressing through the array. In combination with reduced stratification, the homogenization across the lake is likely reduced and hotspots with higher dissolved oxygen and nutrient values occur.

7 Propagating effects on lake ecology

The changes in the lake ecology introduced by the FPV have been the subject of numerous studies. Factors like altered temperature dynamics but also reduced direct solar irradiation have an effect on the water quality. This chapter reflects on published literature related to ecological effects induced by FPV systems and links the results to the quantified effects resulting from the thermodynamic model.

7.1 Light irradiance and microbial organisms

Determining the amount of light that still manages to reach the water surface through the gaps of the FPV system is hard to quantify from drawings alone. However, in a study focusing on another FPV system implemented by GroenLeven, it is assumed that light irradiation of roughly 10% is able to reach the water surface (Obbink, 2023). A reduction in light irradiation of 90% has a notable impact on O_2 producing organisms like phytoplankton and cyanobacteria which can be harmful to marine life. Compared to an open water situation the growth efficiency of these organisms is reduced by 44% and 62% respectively (Obbink, 2023). In addition, the turbidity of the water is correlated to chlorophyll (cells present in algae that perform the photosynthesis process) levels. Turbidity is affected by wind speeds as well as water temperature. The relation between turbidity and chlorophyll is shown in Figure 22. Although the microbial growth varies throughout the season, the continuous presence of the FPV system will have a year-round reducing effect on microbial growth with more constant values lower throughout the year. Concerning Zonnepark Beilen, measurements concerning microbial life in the lake have taken place on three separate occasions in the year 2022. Measurements taken on 29-04-22 indicate that the green algae concentration is on normal levels both in open water and underneath the array ($\sim$20.000 cells/ml for both measurements). Two months later on 27-06-22, measurements indicate that the green algae concentration underneath the array is lower compared to the open water concentration ($\sim$4500 cells/ml vs. $\sim$2600 cells/ml). This is likely the result of reduced light intensity and turbidity, the latter is well explained by Figure 22 The last measurement taken on 29-09-22 shows the same trend concerning the green algae concentrations. With lower concentrations underneath the array compared to open water values ($\sim$6000 cells/ml vs. $\sim$4000 cells/ml). Additionally, blue-green algae (which in high concentrations are toxic) have increased in the open water measurements whereas the sub-array concentrations are significantly lower ($\sim$16.000 cells/ml vs. $\sim$1200 cells/ml) (Pires, 2022). The assumed and measured reduction in microbial growth, especially the blue-green algae, can be seen as a benefit for the water quality at Zonnepark Beilen (Exley et al., 2021; Pires, 2022).

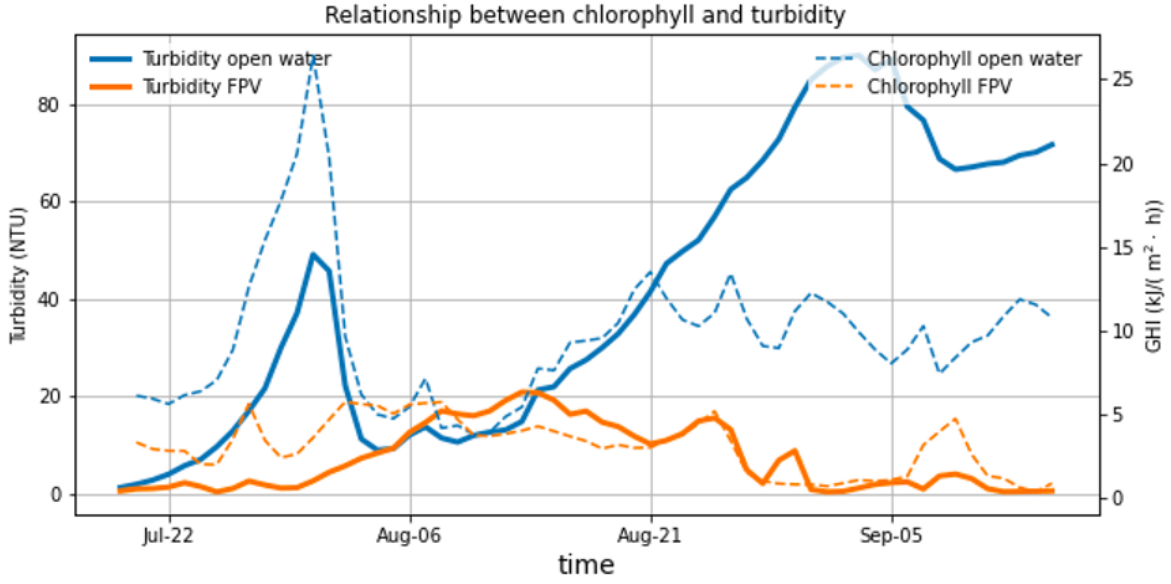

Figure 22: Relationship between chlorophyll and turbidity (Obbink, 2023).

7.2 Dissolved oxygen

Dissolved oxygen is one of the primary indicators of whether an environment is a suitable habitat for nearly all freshwater fish species. In general terms, no fish can survive with dissolved oxygen levels between 0 - 4 mg/l, on the other side all fish species can survive with dissolved oxygen values of 9.5 mg/l or higher (Obbink, 2023). The negative impact of FPV systems on dissolved oxygen is not clearly supported throughout the literature. On one hand dissolved oxygen levels are reduced as oxygen-producing phytoplankton concentrations tend to be lower, as well as stratification is reduced (Obbink, 2023). However in a case study on three lakes, Bax et al. (2023) mention that however a decrease in dissolved oxygen throughout the observed period, FPV systems were not a direct cause. According to the results of the study, seasonal variations resulted in lower dissolved oxygen values during fall and winter, but values never reached a critical level. Additionally, the decreasing trend in dissolved oxygen for the lakes with FPV systems has also been observed in reference observations. According to Elci (2008), dissolved oxygen levels in water are largely dependent on wind speeds at the water surface as a result of reduced stratification. This result is also confirmed by Ni et al. (2016) who mention that stratification and dissolved oxygen levels are strongly correlated.

For Zonnepark Beilen, monthly measurements have been taken for dissolved oxygen values in the lake after FPV installation for the 2022 period. The survey executed by Deltares indicates that throughout the year and at various depths no difference can be seen between dissolved oxygen underneath the array compared to open water, the results are shown in Figure 23 (Pires, 2022). Note that the open system at Zonnepark Beilen is able to supply oxygenated water to the lake, possibly offsetting the reduction of dissolved oxygen which may be introduced by the FPV system.

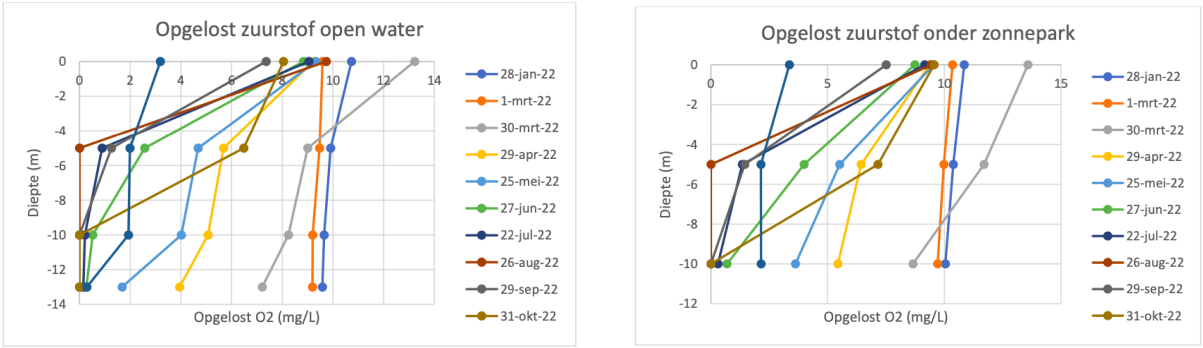

(a) **(b)**

Figure 23: Dissolved oxygen at open water (a) and dissolved oxygen underneath the FPV system (b). Axes: Y= depth (m), X= Dissolved O_2 (mg/l) (Pires, 2022).

As mentioned in section Dissolved oxygen 6.3, the reduced water temperatures and reduced wind speeds which vary across the FPV system will likely cause spatial variations regarding dissolved oxygen levels. However, the measurements taken from Zonnepark Beilen during the implementation of the FPV system prove that no significant changes take place, confirming the results of Bax et al. (2023). Measurements across a longer period of time could provide useful information if this trend remains stable or slowly changes over time.

7.3 Water conductivity

The conductivity of the lake hosting the FPV system can change over time after the array has been placed. This happens because of the suspected leaching of metals in the water, increasing the concentration of metal ions in solution and as a result, increasing conductivity (Obbink, 2023). The report of Lima et al. (2021) investigated the effects of the introduced FPV system at Bomhofsplas, the Netherlands measured the conductivity values underneath the array and at open water across a five-month period. Concluding that there was a 6.6% higher level of conductivity underneath the array compared to the open water value. Data from the thesis of Obbink (2023) also shows a conductivity increase (10.5%) underneath the array compared to the open water conditions. Both results show an increase in conductivity underneath the array. This increase in conductivity can not be explained by water temperature differences or reduced wind speeds. The increased conductivity underneath the FPV system is probably a result of a buffer zone that occurs due to a sheltered climate underneath the array (Lima et al., 2021).

8 FPV economics

As mentioned in the Introduction, FPV systems have an increased price tag compared to GPV systems due to more complicated installation, increased difficulty with cleaning, proprietary floating components, and so on. Based on the results established in this thesis opportunities will be explored to provide opportunities to offset increased costs of FPV systems. Numerous benefits of FPV systems compared to GPV systems were already known, such as higher efficiencies, cleaner solar panels, and water retaining properties on lakes. This chapter will investigate how the thermodynamic and environmental effects can translate into benefits for relevant businesses.

8.1 Fish spawning

A publication from Wageningen University from 2006 mentions that the total CO_2 emissions related to fish spawning in the Netherlands are negligible compared to the overall CO_2 emissions in the Netherlands (Schram et al., 2006). Hence, implementing an FPV system solely for the purpose of offsetting CO_2 emissions is likely not the case. However, the ecological benefits that an FPV system introduces to open-water fish spawns could help with offsetting O&M costs. Installed FPV systems on open water spawning facilities enable local energy generation which can offset partial, if not the total, energy demand of the facility (depending on the facility size). In an analysis established with the cooperation of sportvisserij Nederland benefits and consequences are listed. One of the consequences mentioned is the reduction of light irradiation and algae bloom, which might hinder fish that depend on aqua cultural flora as a food supply. Other arguments focus on installment and maintenance of the arrays which inhibits fishermen from fully utilizing the system (Emmerik, 2019). However, the benefits listed also note opportunities like enhanced living conditions for fish as the array provides shelter against predators (except the fishermen). The underwater structures from the FPV system provide additional space for algae and other organisms that participate in the food chain to cultivate, promoting the fish stock in the lake. Finally, the energy provided by the floating array can provide monetary benefits when sold to the grid surrounding industries, or residential areas. Additionally, the report mentions the possibility of providing energy to pumps to artificially enhance turbidity to mix oxygen into the water if necessary (Emmerik, 2019).

8.2 Water treatment plants

As mentioned in the introduction, FPV systems enable water treatment plants to save costs by significantly reducing water evaporation (Farrar et al., 2022). This concept is already being applied by Evides in the Netherlands, which implement FPV on their water reservoir to make use of the evaporation reduction properties as well as the generated energy to reduce their carbon emissions. Additionally, the reduced algae growth also plays a role for the water treatment plant as it reduces their treatment intensity (Drinkwaterplatform, 2021).

8.3 General benefits for businesses on in-land waters

Looking at the results from the thermodynamic analysis as well as the ecological effects of FPV systems on local environments. The cooling effects of FPV systems on the lake's surface temperature promote water quality by reducing algae growth and reduce evaporation. Improving water retention in lakes, which in the case of the past trend in the Netherlands that features draughts, proves to be a valuable benefit (Wanders et al., 2023). Given the ratio of covered surface area versus FPV area, an 18% evaporation reduction can occur at a lake area coverage of 30%, and covering up 50% can reduce evaporation up to 30% (Bontempo Scavo et al., 2021).

9 Discussion

This chapter aims to examine the implications of the thesis on scientific relevance while addressing the encountered limitations in the execution of the research method. Drawing insights from the results and ensuing discussion, the chapter additionally explores potential future research directions.

9.1 Theoretical implications

9.1.1 Scientific relevance

The method and results of this thesis touched upon a variety of subjects within FPV systems. The initial focus was put on interpreting the thermodynamic effects and the implications on the ecology of the water body, and relevant businesses. However, diving into the topic of thermodynamics, it became clear that a lot of papers do not assess complete arrays in their system boundaries. This means that often, the focus on FPV performance and heating/cooling effects would be limited to either one floating panel or an array < 20 panels (Lindholm et al., 2022; Rahaman et al., 2023). Additionally, in the literature, the thermodynamic effects would be determined from the solar cell perspective and often dismissed changes to the water temperature. Papers that do focus on changes in water temperature tend to focus more on measurements instead of conducting a thermodynamic analysis (Lima et al., 2021; Ilgen et al., 2023; Bax et al., 2023). Conducting the method proposed in this thesis has shown that,in order to take a full-scale system into account the dependence on assumptions and approximated values has notable impacts on the accuracy of the research. Intermediary results indicated that large arrays containing hundreds of panels (on sites like Bomhofsplas, Oudehaske, and Beilen) require a more tailored approach. This means, that site-specific data and measurements on multiple points of an FPV system are necessary to obtain a more accurate result for various parameters. The choice to implement CFD into the method to get better insights into the development of wind speeds underneath the floating array, showed a trend where wind encountering the array showed a rapid decay in its energy with reduced speeds as a result. Wind speeds below the solar panels were notably lower compared to wind speeds at the water level. Concerning heat transfer, this shows that taking the measurements of wind speeds at one level does not justify the generalization of applying the measurements from one or two weather stations and assuming homogeneity across the array. These findings resulted in a different approach taken with the time-series modeling of the thermodynamic effects of heat transfer from the back of the solar panels to the upper water layer, resulting in a more tailored approach Zonnepark Beilen. By subdividing the array in different zones the resolution for changing heat transfer dynamics became higher than when working with measured data from two separate points. Applying CFD on a scale this big in FPV context proved that overall more knowledge regarding wind speed dynamics could prove useful for numerous metrics like module temperatures, performance variability on the array, and environmental impacts.

The results following the thermodynamic analysis show how the FPV system has a cooling effect on the water body as a result of different heat inputs. In comparison to Rahaman et al. (2023)., the focus of the analysis is not specifically on the temperature change of the solar

module but rather on the thermal impact of FPV systems on the water surface. The results show that there is a notable temperature reduction potential for the upper water layer, which is the result of reduced light penetration through the array but also lower wind speeds compared to the lake without the array. While the results agree with results published in other articles, one of the new insights is that impacts of FPV systems do not always occur homogeneously along the array; The reduced wind speeds that occur downwind underneath the array transfer less heat energy from the panels to the water resulting in a more notable cooling effect on the water surface. However, the cooling effect is reversed when looking at module temperatures which are expected to be higher in the downwind part of the array where less heat transfer takes place. The effect of these findings on theoretical studies might be that coefficients might have to be applied to thermodynamic models that account for variations of input parameters along the array (when considering larger arrays). Additionally, quantifying these effects and comparing them with measured effects or applying machine learning algorithms could lead to a better understanding of the key parameters that influence these effects. The indicated effects of heat transfer from the module to the water surface are also expected to result in a voltage drop due to panel heating. The uneven distribution of heat transfer on the array (Figure 16) can cause varying performance output along the array.

Literature suggests that FPV systems have both positive and negative consequences on the environment in which they are applied. Other papers suggest that FPV systems improve water quality by reducing algae bloom potential and lowering the evaporation rate of the lake by reducing water losses during warmer periods. These effects are supported by the results of the CFD and thermodynamic analysis where reduced wind speeds and light irradiation reduce algae concentration through reduced turbidity and lower photosynthetic activity. The reduced evaporation is also confirmed by the reduced wind speeds and relative humidity. Once again, an important notice goes to the variability of the effects that occur along the array, where the once lower wind speeds on the downwind side of the array are likely to induce a bigger effect in the reduction of algae bloom and dissolved oxygen reduction compared to the wind-facing side of the array.

Installing an FPV system on a water body that is related to other economic activities like sports fishing lakes, fish spawning, or a water treatment plant might induce additional economic benefits. This case has already been explored for water treatment plants and has proven fruitful. However, for other economic activities research showed little to no incentives taken for other economic activities yet the potential benefits of reducing grid uptake, CO_2 emission reduction, and improved ecology prove to be useful. The results of economic benefits induced by FPV systems in this paper indicate that both the ecological effects as well as PV performance can be useful for businesses that do not fully occupy space on their waters. These findings highlight a gap in literature focusing on FPV benefits and economics and the potential to offset each other, providing a possible direction for future research, which will be discussed later in this chapter.

9.1.2 Societal relevance

While FPV systems start to attract more attention on both the commercial and public landscape, research is needed to determine the impacts of the FPV system more accurately. The

results presented in this paper introduce new insights that help understand the dynamics surrounding FPV systems. Further understanding the physical dynamics, their impact on large-scale FPV utilities, and the surrounding environment and ecology are important for future implementation of the technology. The potential of FPV in the Netherlands is large and can offset a significant part of the energy generated by fossil fuels, which in turn is beneficial for achieving the climate goals set in the Paris Climate Agreement.

The results presented in this paper can stimulate FPV contractors to look at their current and future plans for FPV systems with the new knowledge regarding the changing dynamics as a result of wind speed depreciation. Conducting the CFD analysis highlighted the importance of specific analyses for sites, structures, and implemented technology as both the structure of the array as well as external factors like incoming wind direction can influence the behavior of the array in terms of panel cooling and optimal string layout. For FPV systems to adopt a more comprehensive analysis regarding environmental aspects and array structure, considering a new project could help to optimize system yield while minimizing ecological impacts.

Water-related businesses can take note of the results indicating that FPV systems do not pose a significant threat to the surrounding ecology. Additionally, the added benefits both financially and to the water quality might incentivize businesses to consider implementing FPV to their water body, which will have a positive impact on the adoption rate of the technology, as well as reduce the business's emissions.

The ecological impacts of FPV system is assessed through the thermodynamic impacts that an FPV system has on the lake, proposing a view from a different angle on how environments are affected. With the results indicating that the ecological effects are mainly beneficial, longer periods of observation might highlight long-term effects. Results from this thesis as well as other publications can provide important insides for policymakers focusing on establishing regulations for FPV systems. Policymakers, for example, can set regulations for systems design that allow for more light penetration or wind speeds to increase dissolved oxygen values.

9.2 Research Limitations

During the execution of the research method, several limitations were encountered during the case study for Zonnepark Beilen, which will be discussed in this section.

9.2.1 Wind speeds and CFD

The dataset obtained for Zonnepark Beilen proved to be very complete with very few data entries missing or needing replacement due to sensor errors. However, due to the size of the array and the level of analysis that has been planned for this thesis project, more data was needed to get the desired results. For the thermodynamic model, accurate data on wind speeds underneath the array were needed for the convective heat transfer. Early on it became clear that approximating the sub-panel wind speeds with the measured wind speeds (above the solar panels) present in the dataset would not generate accurate results. Therefore, it has been decided to re-establish the method of this thesis project to focus on obtaining wind

speeds and dynamics through means of CFD.

While the results of the CFD analysis were deemed successful for this project, numerous limitations occurred during this analysis. First of all, no knowledge was present about CFD except for its existence. This means that information about working principles, establishing 3D models, and setting up analysis all needed to be acquired before the first analysis could be conducted. Due to inexperience, it took trial and error and occasional revisits to get more accurate results for wind speeds and wind dynamics but it is believed that optimal results have not yet been achieved. This limits the accuracy of the results generated by the CFD analysis. These limitations can be prevented in future research by better planning research strategies as well as consulting experts in the field of CFD.

In addition to inexperience in the field of CFD, the obtained results are sub-optimal as a result of computational constraints. As mentioned in section 3.2 the computational limitations resulted in a two-stage approach in the analysis. The computational limitation presented itself in the lack of available memory (32Gb of memory was present while 128Gb was required) in addition to a lack of processing cores as time-out limits have been reached due to computational complexity. Not being able to simulate the entire FPV system resulted in a two-stage analysis, in which results from the primary analysis would be averaged and then used as input for the secondary analysis. While this method showed similar trends as expected it remains an uncertainty and therefore a limitation in terms of the accuracy of the results.

Due to time constraints in both the thesis project as well as simulation time, the CFD analysis has only been executed with the highest measured wind speed (based on hourly average) from the dataset. This means that the wind speeds underneath the array and the decay in wind speeds have been determined for only one wind speed and do not represent the dynamics for lower or higher wind speeds. Running additional analyses with different wind speeds as boundary conditions could have been done but were likely not to reveal any different dynamics as only part of the system could be analyzed.

9.2.2 Thermodynamic model

Limitations were also encountered while establishing the thermodynamic model in this thesis. As mentioned, the dataset proved to be fairly complete for the data that has been recorded. However, an important parameter to determine the heat flow from the back of the panel to the water as well as the evaporation of water was the relative humidity. Data for the relative humidity has been acquired from NASA's climate data services, which works by approximating the relative humidity for one km^2 through satellite imagery and algorithms (NASA, 2023b). NASA's highest accuracy regarding data interval proved to be hourly data. Therefore, the data acquired from Zonnepark Beilen also had to be adjusted to an hourly interval. While the relative humidity is determined with some degree of accuracy, having the data measured directly from the weather stations present at Zonnepark Beilen would have heightened accuracy of the study. In addition, the temperature results from the thermodynamic model are indicative but are based on one-year data. For more comprehensive and accurate results, the temperature data will need to be extrapolated for the lifetime of the system to get a better idea of the implications of the FPV system on water temperatures.

9.3 Opportunities for further research

This section discusses the opportunities for future research based on the results and prior discussion of this master's thesis.

9.3.1 CFD

The CFD analysis conducted in this thesis project created valuable insights and visuals that contributed to a better understanding of the wind speed dynamics surrounding a FPV system. Yet, the CFD analysis for this thesis has only been capable of simulating the effects for a small part of the total array (0.9%) in one go. The second analysis was run with sub-optimal inputs concerning accuracy. As the results of this study highlight, there is a notable difference in temperature dynamics along the FPV system which is mainly dependent on wind speeds and wind dynamics. Future research focusing on mapping complete floating arrays on wind dynamics but also heat transfer could provide valuable information on the impact of FPV systems on the host water bodies, and also improve array design. CFD analysis results could serve as an argument to go for arrays allowing for better wind pass-through to enhance cooling and heat transfer, or possibly denser configurations to optimize for space and reduce evaporation by limiting evaporation. As CFD analyses required significant computational capabilities, it is suggested to set up systems in a supercomputer environment to allow for acceptable simulation times and ensure the possibility of simulating full-scale systems.

9.3.2 Tilt angle variation

Using CFD to determine wind and temperature dynamics is useful to determine heat transfer from solar panels to their surroundings. In addition, a thorough analysis can be done focusing on system design. Research focusing on the change in force, heat transfer, and wind speeds based on varying module heights and tilt angles could provide useful insights for optimizing the spatial layout of FPV systems.

9.3.3 Economic impacts

As mentioned in section 1.3, the initial aim for this thesis was to quantify the impacts of an FPV system on the environment and how this has economic impacts on businesses. While this paper touches on the subject of economic impacts and possibilities, a quantitative result remains absent. For future research, it can be interesting to quantify the economic effects induced by FPV systems. Quantifying these effects can provide valuable insights regarding the LCOE, O&M, and CAPEX of both FPV systems and businesses because, as mentioned costs made by businesses can possibly be offset by the introduced FPV system. Results presented by research focusing on this subject can help business owners but also contractors involved with FPV systems with their decision-making process, but also provide scientific insights on how these economic effects can be further exploited.

9.3.4 Water temperature analysis

The results of the thermodynamic analysis show a small decline in water surface temperature throughout the year. The survey conducted at Zonnepark Beilen by Pires (2022) indicated that hardly any temperature changes have been measured across the lake. However, future research focusing on water temperatures is suggested as the FPV system at Beilen is relatively young at 2.5 years and long-term effects could still be unknown. Additionally, further assessment targeting various depths can give a broader view of the thermal dissipation in the lake providing a broader insight into potential effects on local ecology.

10 Conclusion

This section will provide answers to the established research questions in section 1.3, During this thesis project, we shifted our focus more toward thermodynamics, as it's a key part of our study. This meant we spent less time on the financial aspects of floating solar panels, which was our original plan. We did this to make sure we explored thermodynamics well within our deadline. In addition, at the beginning of the research phase, it was not clear that access to expensive CFD software would be possible with a student license. After realizing this opportunity, the choice has been made to further investigate wind speed dynamics utilizing Autodesk CFD software. This resulted in a choice to focus less on the financial aspects of FPV systems and businesses related to in-land waters, which initially was the main focus of this thesis project.

To answer the main research question *"What are the added economic benefits of an FPV system for businesses that are reliant on in-land water bodies and how are these, in turn, beneficial for FPV implementation?"* the sub-research questions will first be addressed to provide context and background information before reaching a conclusion.

The first sub-research question states: *"What are the thermodynamic effects of FPV systems on in-land water bodies?"*. This question is answered by combining the results of the CFD and thermodynamic analysis. The main impacts of FPV systems on in-land water bodies are reduced wind speeds and a cooling effect introduced by a reduction of direct sunlight entering the water body. While the reduced wind speeds and light irradiation are already known and could be expected. In addition to reduced wind speeds, heat transfer from the back of the solar panels to the water surface also takes place, albeit this also depends on wind speeds. The magnitude and distribution of these effects remained relatively unknown. Depending on the wind direction and speed, heat transfer underneath the array is mainly present on the side of the array directly facing the wind, resulting in more heat transfer from the back of the panels to the water surface. Sides of the array that are down-wind or obstructed feature lower wind speeds and thus lower heat transfer rates. In the case of Zonnepark Beilen, these effects translate to a notable cooling effect introduced by lower heat input into the water body, albeit the magnitude of the effect is location-dependent.

These insights can now be used to answer the second sub-research question: *"How do these effects translate into environmental impacts in the water body?"*. The reduced wind speed and temperature impact the lake environment in a couple of ways, but in general, do not induce significant threats to the environment. Microbial growth in the water body is reduced but not completely stopped improving water quality. Additionally, stratification may be reduced as a direct result of reduced wind speeds underneath the array, having a side effect that less oxygen dissolves into the upper water layer. In the case of Zonnepark Beilen (see section 7.1) effects on turbidity and algae bloom were noticeable but differences in dissolved oxygen have not been confirmed as a result of introducing the FPV system for this case study due to the open system nature of the lake. However, reduced dissolved oxygen levels have been measured in other water bodies containing FPV systems, indicating that this effect is rather location-specific and might require more attention. Introducing the FPV systems slightly increases the water's conductivity, these effects however are not significant enough to pose any environmental threats. Note that the case study for Zonnepark Beilen is slightly different

due to its open system having an incoming and outgoing flow of water at the south side of the lake compared to closed system water bodies.

With the thermodynamic and environmental impacts identified, the last sub-research question can also be answered: *"How do these thermodynamic and environmental effects translate to economic impacts for businesses?"* As mentioned earlier, economic impacts have only been assessed by a qualitative approach, the identified potentials are only an indication and might be only a handful of all possible effects. First of all, the energy-generating capabilities are an obvious benefit for businesses as they provide the opportunity to reduce electricity costs and offset carbon emissions produced by potential businesses like fish spawners, sports fishing facilities, and water treatment plants. The reduced wind speeds and lower water temperatures additionally have a water-containing effect by reducing evaporation from the water body, which combined with the reduced algae bloom, improves water quality, reduces the need for additional water treatment, and prevents additional costs.

With the provided answers to the sub-research questions, the answer to the main research question is formulated as follows: Economic benefits potentially induced by FPV systems come in various opportunities. Electricity generated by the array can used and/or sold to the grid resulting in either savings or additional income for the respective business implementing the system. Additionally, increased sustainability can improve the business's sustainable image and perception to the public as well as future-proof business operations. Effects like reduced algae bloom, water retention due to reduced evaporation, and reduced turbidity improve water quality which in turn can be beneficial for marine life and businesses dependent on sufficient water quality standards, by for example, reducing water treatment frequency and costs. While these results are not quantified, they have the potential to save or prevent costs that have to be made by businesses for maintenance or general operating efforts. Businesses contemplating on installing an FPV system should consider these economic benefits as in turn, the saved and/or prevented expenses can offset the CAPEX of an FPV system, improving implementation rates and sustainable energy production.

11 Acknowledgements

During this thesis project, numerous points made me struggle and feel lost, especially after taking a different route in the methodology than I first intended. Therefore, I would sincerely like to thank my supervisors Dr. Sara Mirbagheri Golroodbari and Annanta Kaul for their continuous support and availability for my questions and in sharing their insights. I feel proud of this thesis report and would not have been able to provide the same quality without them.

References

Ahmed, N., Thompson, S., and Glaser, M. (2019). "Global Aquaculture Productivity, Environmental Sustainability, and Climate Change Adaptability". In: *Environmental Management* 63 (2), pp. 159–172.

Baltazar, J. C. and Claridge, D. E. (2006). "Study of cubic splines and fourier series as interpolation techniques for filling in short periods of missing building energy use and weather data". In: *Journal of Solar Energy Engineering, Transactions of the ASME* 128 (2), pp. 226–230.

Bax, V., van de Lageweg, W. I., Hoosemans, R., and van den Berg, B. (2023). "Floating photovoltaic pilot project at the Oostvoornse lake: Assessment of the water quality effects of three different system designs". In: *Energy Reports* 9, pp. 1415–1425.

Bontempo Scavo, F., Tina, G. M., Gagliano, A., and Nižetić, S. (2021). "An assessment study of evaporation rate models on a water basin with floating photovoltaic plants". In: *International Journal of Energy Research* 45.1, pp. 167–188.

Cao, L., Halpern, B. S., Troell, M., Short, R., Zeng, C., Jiang, Z., Liu, Y., Zou, C., Liu, C., Liu, S., Liu, X., Cheung, W. W., Cottrell, R. S., DeClerck, F., Gelcich, S., Gephart, J. A., Godo-Solo, D., Kaull, J. I., Micheli, F., Naylor, R. L., Payne, H. J., Selig, E. R., Sumaila, U. R., and Tigchelaar, M. (2023). "Vulnerability of blue foods to human-induced environmental change". In: *Nature Sustainability 2023*, pp. 1–13.

CBS (2023). *Aandeel hernieuwbare energie in 2022 toegenomen naar 15 procent (Share of renewable energy in 2022 increased to 15 percent)*.

Chowdhury, G., Haggag, M., and Poortmans, J. (2023). "How cool is floating PV? A state-of-the-art review of floating PV's potential gain and computational fluid dynamics modeling to find its root cause". In: *EPJ Photovoltaics* 14.

Cochrane, K., Young, C. de, Soto, D., and Bahri, T. (2009). "Climate change implications for fisheries and aquaculture. Overview of current scientific knowledge. FAO Fisheries and Aquaculture Technical Paper No. 530." In: *FAO Fisheries and Aquaculture Technical Paper* (December 2009), p. 212.

Cooperatie Project de Mussels (2023). *OVER DE MUSSELS*. URL: https://www.demussels.nl.

Denhard, A., Bandyopadhyay, S., Habte, A., and Sengupta, M. (2021). *Evaluation of Time-Series Gap-Filling Methods for Solar Irradiance Applications*.

Dörenkämper, A. M., Jong, M. D., Villa, S., Aken, B. V., Apaydin, O., and Biesheuvel, W. (2022). "AC-Yield: An investigation into cooling of modules in floating PV systems and light penetration in land-based solar parks." In: June, pp. 1–44.

Drinkwaterplatform (2021). *Drijvende zonnepanelen: PWN en Evides zijn de Europese koplopers*.

Elci, S. (2008). "Effect of thermal stratification and mixing on reservoir water quality". In: *Limnology* 9, pp. 135–142.

Elkholy, A. and El-Ela, A. A. A. (2019). "Optimal parameters estimation and modelling of photovoltaic modules using analytical method". In: *Heliyon* 5 (7).

Emmerik, W. A. M. van (2019). "Notitie. Drijvende zonneparken. Vissen, sportvisserij en ecologie." In: *Sportvisserij Nederland, Bilthoven*.

Essak, L. and Ghosh, A. (2022). "Floating Photovoltaics: A Review". In: *Clean Technologies* 4 (3), pp. 752–769.

Exley, G., Hernandez, R. R., Page, T., Chipps, M., Gambro, S., Hersey, M., Lake, R., Zoannou, K. S., and Armstrong, A. (2021). "Scientific and stakeholder evidence-based assessment:

Ecosystem response to floating solar photovoltaics and implications for sustainability". In: *Renewable and Sustainable Energy Reviews* 152, p. 111639.

Farrar, L. W., Bahaj, A. S., James, P., Anwar, A., and Amdar, N. (2022). "Floating solar PV to reduce water evaporation in water stressed regions and powering water pumping: Case study Jordan". In: *Energy Conversion and Management* 260, p. 115598.

Folkerts, W., Sark, W. van, Keizer, C. de, Hooff, W. van, and Donker, M. van den (2017). *ROADMAP PV Systemen en Toepassingen*.

Golroodbari, S., Fthenakis, V., and Sark, W. G. van (2022). "1.32 - Floating Photovoltaic Systems".

Golroodbari, S. and Sark, W. V. (2023). *Do floating PV systems warm up the water body?*

Gorjian, S., Sharon, H., Ebadi, H., Kant, K., Scavo, F. B., and Tina, G. M. (2021). "Recent technical advancements, economics and environmental impacts of floating photovoltaic solar energy conversion systems". In: *Journal of Cleaner Production* 278.

Green, M. A., Dunlop, E. D., Yoshita, M., Kopidakis, N., Bothe, K., Siefer, G., and Hao, X. (2023). "Solar cell efficiency tables (version 62)". In: *Progress in Photovoltaics: Research and Applications*.

GroenLeven (n.d.). *Drijvend zonnepark Sekdoornse plas - groenleven.nl*.

Heiskanen, J. J., Mammarella, I., Ojala, A., Stepanenko, V., Erkkilä, K.-m., Miettinen, H., Sandström, H., Eugster, W., Leppäranta, M., Järvinen, H., Vesala, T., and Nordbo, A. (2015). "Journal of Geophysical Research : Atmospheres". In: pp. 7412–7428.

IEA (2022). *Renewable Energy Market Update 2022*.

Ilgen, K., Schindler, D., Wieland, S., and Lange, J. (2023). "The impact of floating photovoltaic power plants on lake water temperature and stratification". In.

Ji, Q., Li, K., Wang, Y., Feng, J., Li, R., and Liang, R. (2022). "Effect of floating photovoltaic system on water temperature of deep reservoir and assessment of its potential benefits, a case on Xiangjiaba Reservoir with hydropower station". In: *Renewable Energy* 195, pp. 946–956.

Jiang, Q., Bhattarai, N., Pahlow, M., and Xu, Z. (2022). "Environmental sustainability and footprints of global aquaculture". In: *Resources, Conservation and Recycling* 180, p. 106183.

Kadaster (2023). *Kwartaalbericht agrarische grondmarkt 2022-4*.

Khokhar, M. Q., Zahid, M. A., and Kim, J. (2020). "A Review on Floating Photovoltaic Technology (FPVT)". In.

Kjeldstad, T., Lindholm, D., Marstein, E., and Selj, J. (2021). "Cooling of floating photovoltaics and the importance of water temperature". In: *Solar Energy* 218, pp. 544–551.

Kumar, M., Niyaz, H. M., and Gupta, R. (2021). "Challenges and opportunities towards the development of floating photovoltaic systems". In: *Solar Energy Materials and Solar Cells* 233.

Lima, R. L. de, Paxinou, K., Boogaard, F. C., Akkerman, O., and Lin, F. Y. (2021). "In-situ water quality observations under a large-scale floating solar farm using sensors and underwater drones". In: *Sustainability (Switzerland)* 13.11.

Lindholm, D., Selj, J., Kjeldstad, T., Fjær, H., and Nysted, V. (2022). "CFD modelling to derive U-values for floating PV technologies with large water footprint". In: *Solar Energy* 238.April, pp. 238–247.

Mackey, A. P. and Berrie, A. D. (1991). "The prediction of water temperatures in chalk streams from air temperatures". In: *Hydrobiologia* 210.3, pp. 183–189.

NASA (2021). *Navier Stokes equations*. URL: https://www.grc.nasa.gov/www/k-12/airplane/nseqs.html (visited on 10/17/2023).

NASA (2023a). *Data Sources*. URL: https://power.larc.nasa.gov/docs/methodology/data/sources/.

NASA (2023b). *Relative Humidity*. URL: https://power.larc.nasa.gov/docs/methodology/meteorology/relative-humidity/.

Nations, U. (2022). *Netherlands Population*.

Ni, X., Huang, D., Zeng, D., Zhang, T., Li, H., and Chen, J. (2016). "The impact of wind mixing on the variation of bottom dissolved oxygen off the Changjiang Estuary during summer". In: *Journal of Marine Systems* 154. Changjiang (Yangtze River) Estuary and Adjacent Marine Environment, pp. 122–130.

Obbink, Y. (2023). "Environmental and technological advantages and disadvantages of Floating Photovoltaics in the Netherlands". Master's thesis. Utrecht University.

Pires, M. D. (2022). "Monitoring drijvende zonnepark Beilen". In.

Rahaman, M. A., Chambers, T. L., Fekih, A., Wiecheteck, G., Carranza, G., and Possetti, G. R. C. (2023). "Floating photovoltaic module temperature estimation: Modeling and comparison". In: *Renewable Energy* 208, pp. 162–180.

Schram, E., Sereti, V., Buisonje, F. D., Eding, E., and Ellen, H. (2006). "Institute for Marine Resources and Ecosystem Studies Inhoudsopgave". In: p. 90.

Silva, G. D. P. D. and Branco, D. A. C. (2018). "Impact Assessment and Project Appraisal Is floating photovoltaic better than conventional photovoltaic? Assessing environmental impacts Is floating photovoltaic better than conventional photovoltaic? Assessing environmental impacts". In.

Solar 365 (2023). *De potentie van drijvende zonnepanelen*. URL: https://www.solar365.nl/nieuws/de-potentie-van-drijvende-zonnepanelen-65A7ACAF.html#:$%5Csim$:text=In%202022%20was%20er%20230,binnenwateren%20en%20op%20de%20Noordzee. (visited on 12/15/2023).

Statista (2023a). *Average greenhouse gas emissions per kilogram of major food products worldwide*.

Statista (2023b). *Monthly prices for beef worldwide from January 2014 to June 2023*.

TNO (n.d.). *Drijvende zonnepanelen — TNO*.

Ven, D. J. van de, Capellan-Perez, I., Arto, I., Cazcarro, I., Castro, C. de, Patel, P., and Gonzalez-Eguino, M. (2021). "The potential land requirements and related land use change emissions of solar energy". In: *Scientific Reports 2021 11:1* 11 (1), pp. 1–12.

Wanders, N., Vliet, M. van, Sasidharan, R., Kleinhans, M., Gilissen, H. K., and Jones, E. (2023). *Heat and draught in the Netherlands*.

Zaini, N., Kadir, M. Z. A., Izadi, M., Ahmad, N., Radzi, M., and Azis, N. (2015). "The Effect of Temperature on a Mono-crystalline Solar PV Panel". In.

Zomerdijk, T. (2018). *Weerstand tegen zonneparken*.

12 Appendix A

In addition to the planes used to highlight the wind dynamics, two path trace figures have been extracted from the model. The path traces show how a dot grid placed at the inlet of the air box develops around the array. The path traces on top of the array (Figure 25) show how the wind speed picks up in the 'valleys' of the array where two strings meet with the east and west-facing panels. The valleys deflect the wind from its original direction and make the wind align more with the northern direction facing the top of the array. Looking at the bottom of the figure it can also be seen that wind traces emerge from underneath the solar panels. The dynamics of the wind underneath the panels are better highlighted in Figure 24. Here it is also visible that the wind gets deflected from its original direction and heads more north towards the top of the array. However, it can be seen that traces starting from the most right-facing string are more likely to keep their original momentum when facing the array at the rack height instead of entering through the face of the string. One important aspect that can be noted from Figure 25 is that looking at the 'West' side of the array (bottom right in the figure), the wind continues to enter the array at rack height which enables the wind to maintain better momentum and therefore retain a higher wind speed. This has to be taken into account when west-facing strings are assigned wind speeds in the thermodynamic model.

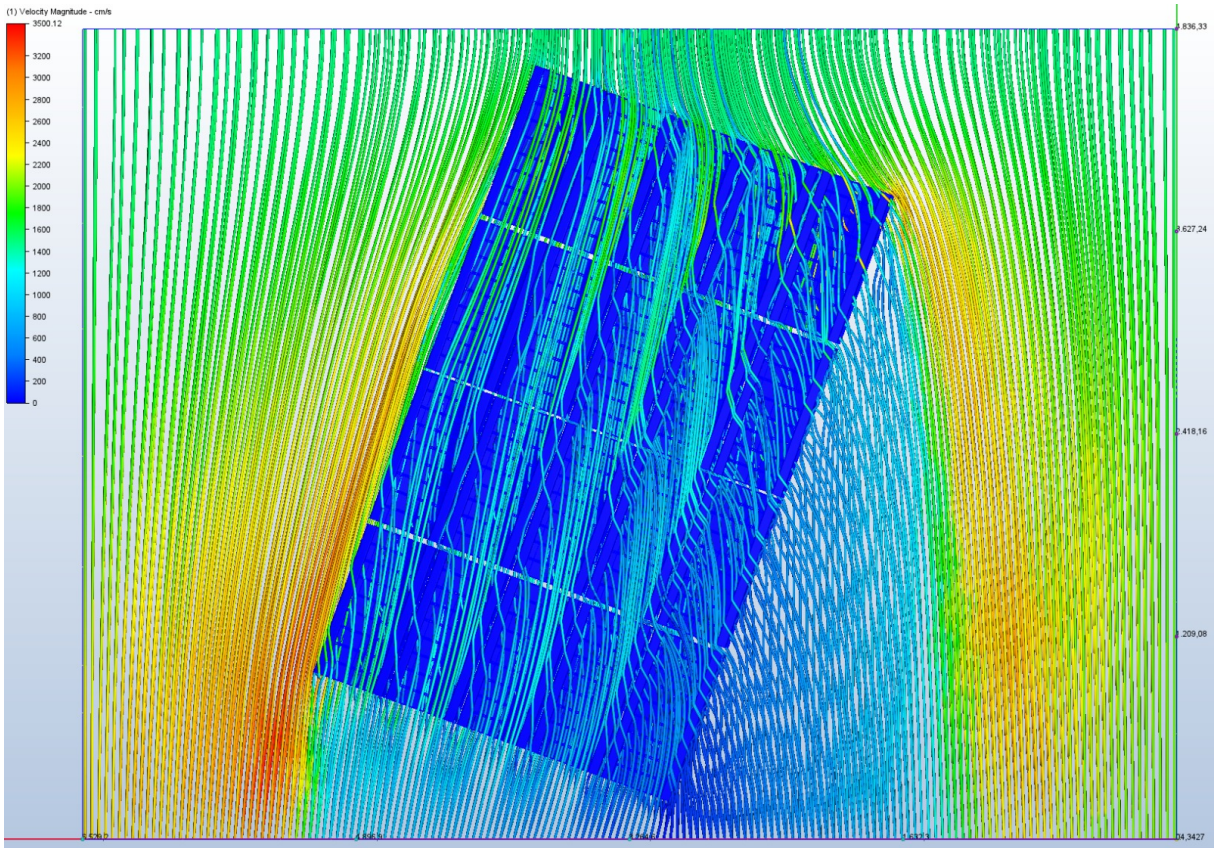

Figure 24: Path development underneath the array for step 1

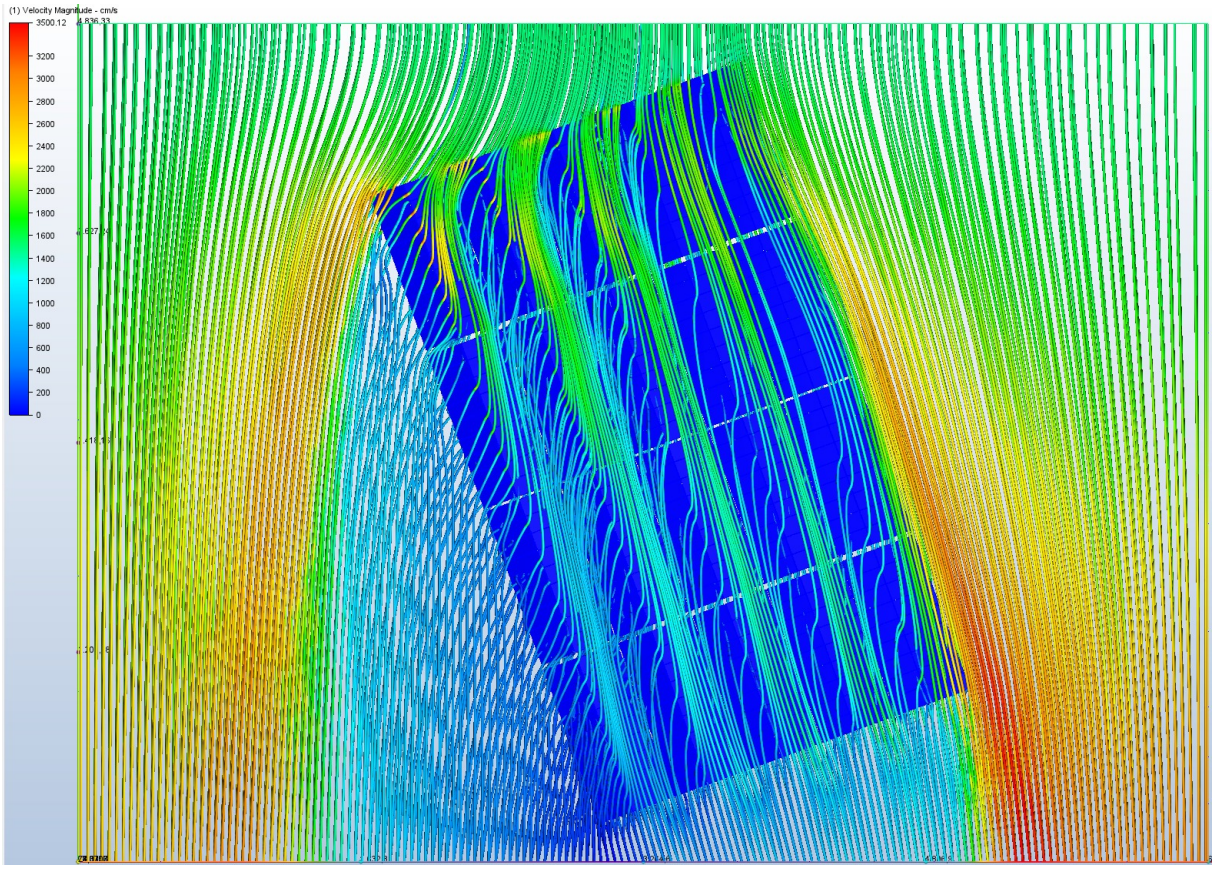

Figure 25: Path development on top the array for step 1